An improved method to calculate paediatric skull fracture threshold

Nagarajan Rangarajan, John DeRosia, John Humm.
The Medical College of Wisconsin
USA

Danny Thomas, MD , John Cox, MD
The Children's Hospital, Milwaukee
USA

Paper Number 13-0211

ABSTRACT

There is a need to better understand the threshold for paediatric skull fracture. Historically, drop tests of cadaver heads have been used to estimate thresholds. However, societal and ethical considerations prevent tests with child cadavers. Therefore, researchers have attempted to estimate the threshold by scaling adult tolerance data. Recent work suggests that mass and material scaling of adult tolerance data is insufficient to develop robust estimates of paediatric skull fracture tolerance. Researchers have also attempted to develop finite element models to estimate skull fracture tolerance. These models require that both geometry and material properties of the skull and brain be known, but, while detailed geometry is known, lack of experimental material test data prevents development of reliable finite element models. This paper describes development of a method to estimate skull fracture tolerance using fall data collected in emergency room. The method depends on the observation that width of force versus time pulse recorded in head drop tests onto a given surface does not vary with height of fall or the mass of head. This observation is supported by analyzing data from adult cadaver head drop tests onto 50mm thick 90 Shore D, and 40 Shore D rubber pads. Next, data from neonatal head drop tests are used to estimate pulse width when an infant head is dropped onto a steel plate. This pulse width is used together with child fall data collected at the Children's Hospital, Milwaukee to estimate forces needed to cause a simple linear fracture in an infant head. This paper describes the procedures used to obtain anthropometric data and fall data such as height of fall and type of surface that the head contacted. This physics based method can be used to analyse child fall data relatively easily to obtain robust estimates of child skull fracture.

INTRODUCTION

Paediatric skull fracture threshold is an important variable needed to design a number of child protective devices such as helmets, child seats and children's playground surfaces. Historically, skull fracture thresholds are estimated from drop tests of Post Mortem Human Subjects [PMHS] heads. Drop tests were the used to estimate adult skull fracture threshold levels. However, societal and ethical considerations prevent testing with child PMHS. Therefore, researchers have attempted to use scaling laws to estimate paediatric skull fracture tolerance levels from adult skull fracture tolerance levels [Irwin and Mertz, 1997, Melvin, 1995]. Initially, mass scaling was used but it was soon realized that differences in structure of the adult and child skull, and material properties would require that material properties also be scaled in the estimation of threshold [Thibault and Margulies, 1999].

Paediatric skull fracture threshold is also of interest to clinicians and in the field of forensic medicine. In many instances, physicians and law enforcement personnel are required to determine whether head injury is a result of an accident or abuse. Tarrantino et al [1999] reported that unintentional falls were the leading cause of non-fatal injury in infants less than a year old. Linear skull fractures are seen 58% of the time in accident cases [Reece and Sege, 2000] found that linear fractures were much more common than complex fractures in accident cases and occurred in 54% of the cases.

Prange, et al [2004] conducted head drop tests using 3 neonate heads. The heads were dropped from 15 and 30 cm heights and the objective of the tests were not to cause fracture. Weber [1984, 1985] conducted whole body child PMHS drop

tests in which child PMHS were dropped onto surfaces of varying stiffness such as tile, carpet, and softer surfaces. The drop height was standardized at 82 cm and he found that all drops onto stiff tile floor resulted in simple linear fractures. Weber did not describe the storage procedures for the PMHS specimens and the specimens were not instrumented.

Researchers have attempted to develop Finite Element [FE] models of varying degrees of sophistication to study the problem of skull fracture [Coats, 2007, Wagner, 2012, Klinich,2002, Roth, 2010]. Development of reliable FE models requires that anthropometry and material properties of the skull and brain be known. Current developments in scanning technology make it possible to obtain fairly accurate information about geometry of the paediatric skull but inability to conduct tests with paediatric specimens make it difficult, if not impossible to accurately prescribe material properties in FE models. Because of these problems, FE models can at best be used as a trend predicting tool. Reliable FE models generally require powerful computers to exercise them and considerable time may have to be devoted to develop input data sets and to analyse the output. This can be time consuming and expensive.

The aim of this paper is to develop a simple, physics based method to estimate paediatric skull fracture tolerance. Our aim was to develop a method that could be installed in the form of spreadsheet programme on PCs, and, which would yield estimates for skull fracture tolerance in terms of peak loads. We feel that this method can be used to analyse fall data as they are obtained and to form robust initial estimates of skull fracture tolerance.

The proposed method depends on the observation that width of force-time pulse in head drop tests does not vary significantly with changes in contact velocity [drop height] or mass. Therefore, it is possible to use currently available data from a limited set of child PMHS tests [Prange,et al. 2002] in conjunction with impulse-momentum theorem to develop reliable estimates of paediatric skull fracture thresholds.

The work described in this paper is split into 4 parts listed below:

1. Confirmation of invariance of pulse width for adult PMHS tests for head drop tests onto Shore 40D and 90D pads from various drop heights. Data used in this confirmation process will be described in the METHODOLOGY section. Results will be discussed in the RESULTS section.
   This paper assumes that the Impact force – Time waveform in a head drop test is tri-angular in shape. With this assumption, the impulse-momentum theorem will be invoked to estimate peak impact force for a given change in momentum of the head. Estimated peak force will be compared with measured peak force for each PMHS test. Comparisons will be presented in the RESULTS section.
2. Collection of prospective data in the Emergency Room [ER] from paediatric patients reporting with linear skull fractures. Procedures used to collect data will be discussed in the METHODOLOGY section.
3. Once the invariance of pulse width is confirmed, we will assume that this will hold for child PMHS head drop tests onto steel plates. Data from tests conducted by Prange, et al [2004] will be analysed in the METHODOLOGY section to reconfirm this principle for infant PMHS head drop tests. An estimate of pulse width will be obtained from Prange [2004].
4. ER data collected includes one case of a 4-month old child who fell onto concrete floor resulting in a simple linear fracture. It is assumed that the pulse width obtained from neonate head drop tests onto to steel plates is applicable to this fall. Impact force resulting from the fall will be calculated invoking the Impulse-Momentum theorem for the known fall height, fall surface, and anthropometry of the infant, once again assuming that the Force-Time curve has a tri-angular shape. This process will be discussed in the RESULTS section.

METHODOLOGY

This section will describe procedures used to confirm the hypothesis of invariant pulse width and to collect child fall data in the Emergency Room [ER].

Confirmation of Hypothesis Regarding Pulse Width - Analysis of Adult Head Drop Test Data

The first objective of this study was to confirm the observation that pulse width of the force vs time curve in head drop tests does not vary appreciably with reasonably large changes in drop height [impact velocity] and mass of the head as long as the head is dropped onto the same contact surface. Lateral head drop tests conducted by Yoganandan et al [2004] were analysed to confirm this hypothesis. In Yoganandan [2004], isolated heads of Post Mortem Human Subject [PMHS] were freely dropped onto 50.8 mm thick rubber pads. PMHS skulls were dropped onto their laterla aspect. Rubber pads with Shore durometer values of 40D and 90D were used. Drop heights were varied in steps from 305 mm to 2134 mm. In this study data from tests where no fracture was observed were used. We provide a brief description of the test methodology, for a fuller description of the PMHS preparation and test methodology, please see Yoganandan [2004].

PMHS heads were isolated at the level of the occipital condyles and further prepared by the replacement of the intercranial content by Sylgard gel that closely mimics the density and mechanical properties of the human brain. Pretest radiographs and computed tomography (CT) scans ((Somatome Plus, Siemens Inc., Germany) were taken of each skull. Tri-axial accelerometers were mechanically fixed to the skull and after each test, the mounting of all instrumentation was checked to assure it remained rigidly attached. Each skull was measured and weighed before and after instrumentation was attached. The skulls were dropped onto a six axis load cell padded with flat elastomeric 40- and 90-durometer material (50 mm thickness). The mid-sagittal plane of the specimen was aligned at an angle of approximately 10 degrees with respect to the horizontal plane such that the impact occurred to the left tempro-parietal region. Each specimen was dropped from successively increasing heights until either fracture or the limits of the load cell was reached. The heights were 305, 610, 914, 1219, 1524 and 2438 millimetres. After each drop the specimen was radiographed and examined for evidence of skull fracture. Biomechanical response data were gathered using a digital data acquisition system according to SAE J 211 specifications at a sampling frequency of 12.5 kHz.

Table 1.
Specimen Data

ID	Age, Years	Height, cm	Weight, kg	Head Weight, kg	Gender
1500	56	178	96	4.37	M
1600	30	163	41	3.52	F
1700	71	169	81	3.72	M
1800	44	178	91	4.48	M
1900	59	182	100	4.52	M
2200	74	178	51	3.8	M
2300	81	157	60	3.24	F
2400	67	168	87	3.66	F

Peak vertical force, Fz and pulse width for each PMHS test were obtained by analysing data from the load cell. The pulse width was calculated as the time between a threshold of 5% of peak values.

The following data were abstracted from test results:

1. PMHS ID number
2. PMHS head mass
3. PMHS gender
4. Force – Time data from the load cell.

All data were entered into a Excel spreadsheet for further analysis.

Collection of Child Fall Data

This Section will describe the procedure used to colleact child fall data in the ER.

Overview

This was a case-control study. We recruited children ages 0 to 3 years old (36 months) who present to Children's Hospital of Wisconsin's Emergency Department/Trauma Center (EDTC) within 48 hours of witnessed blunt head injury. Details of the fall such as the circumstances, estimated height, and nature of surface contacted were obtained from an adult witness for eligible subjects. In addition, anthropomorphic data (height, weight, and head circumference) were also obtained. All daa for eligible participants were recorded in standardised data sheets in the Emergency Department and Trauma Center [EDTC] database.

Participants

Participants were recruited from the Children's Hospital of Wisconsin Emergency Department and Trauma Center [EDTC]. All eligible patients with witnessed head injury due to a fall were evaluated within 48 hours in the EDTC during the study period. Screening occurred based on the availability of physician co-investigator. In order to ensure that no patients were missed during screening, all patients with an injury to the head (direct force or transmitted force) were identified by related chief complaints noted on the EDTC tracking board and were screened for eligibility by the EDTC research assistants. Chief complaints included any description of an injury to the head or an associated mechanism with the potential to have sustained direct force to the head (e.g., "concussion," "head injury," "laceration," or "fall"). If screened patients met inclusion/exclusion criteria based on medical record and discussion with the treating medical team, they were recruited for participation in a study on pediatric head injury. If the patient agreed to study participation, the research assistants then contacted the physician co-investigator to complete the Structured Assessment of Injury. Additionally, anthropomorphic data not already collected (height and head circumference) per usual EDTC processes was collected.

Inclusion criteria

EDTC patients ranging in age from 0 to 3 years were eligible who presented to the EDTC within 48 hours of a reported injury involving the head secondary to a fall were eligible to particpate in the study.

Exclusion criteria

These included conditions that would alter the dynamics of the injury (e.g. helmet use, metabolic bone disease, known intracranial disease or injury), mechanisms that were not fall related or prevented a valid assessment of injury details (unwitnessed event, inability to verbally contact adult who witnessed event, physician concerned for inflicted trauma, or non-English speaking patient/family).

Patients were recruited in two groups: children with linear skull fractures confirmed on imaging and children without skull fracture (either scalp hematoma but no skull fractures seen on imaging or children with scalp lacerations and no suspected fracture). For this preliminary report, we recruited 4 patients in 6 months.

Setting

The study took place at the Children's Hospital of Wisconsin Emergency Department/Trauma Center (EDTC). The EDTC is certified by the American College of Surgeons as a Level I Pediatric Trauma Center. It is the only freestanding Level 1 pediatric trauma center in Wisconsin. The primary catchment area for the Trauma Center includes Milwaukee County and six other counties in southeastern Wisconsin. The total population of the seven-county area is 1,960,289 people, of which 505,279 are children under 22 years of age. Of this total, 48% live within Milwaukee County. The total area is 2,622 square miles (including 242 square miles in Milwaukee County). The secondary catchment area includes 12 additional counties in Wisconsin and northern Illinois. The EDTC has 60,979 visits annually, with a patient age range of 0–22 years old, 54% male, and a racial distribution of 37% Caucasian, 42% African American (AA), and 15% Hispanic non-AA.

From 2002-2008, there were a total of 419 skull fractures in children under the age of three years at CHW, an average of 60 per year (range 45 to 77, with no obvious trend over time). In 2008, there were a total of 1354 blunt head injuries without skull fracture (1075 scalp lacerations and 279 blunt head injuries without skull fracture or intracranial injury) in children under the age of three. Racial and gender distributions were similar to the general EDTC population. Falls predominate as a cause of injury in these patients, regardless of race and gender. EDTC research assistants staff the department 15 hours a day, 5 days a week, during peak census hours. Our physician co-investigator was available for a total of 4 calendar months distributed over the study period. Our experience is that most patients younger than 3 with blunt head injury present to the ED during peak census hours.

ER Data Collection Methods

Structured Assessment of Injury (SAI): Witnesses to the injury were asked to complete an injury survey. The survey was administered as a structured interview by the physician investigator. The assessment collected anthropomorphic data including height, weight, head circumference, and points of impact or injury. Points of impact were documented via body map and, when permitted, digital photographs. Witness' detailing of the fall were documented including, but not limited to, height of the fall, position of the body during the fall, objects struck while falling, and position of the body after

the child came to rest. In addition, a researcher went to the location of the fall and collected data such as fall height, full surface material, etc. Measurements of relevant objects (i.e. height of furniture from which the patient fell) were taken using a standard measuring tape. As in the case of patients who fell from a caretaker's arms, the caretaker assumed the approximate position they were in when the patient fell, and relevant measurements (i.e. height of arm) were taken. When applicable, drawings were used on the SAI to accurately demonstrate the mechanism of the fall. When visiting the site of the fall, photographs were taken to corroborate the witness' description of the fall. Data related to immediate injury outcomes was obtained from the patients' medical record. These data included digital imaging, when applicable. Any available imaging data was collected and converted for use in the project.

Data collected in ER-Study subject

4 patients were eligible for inclusion in the study. Out of these, only 1 fell onto a stiff surface. This patient was a 4-month old, male, 0.66 m tall, and weighing 7.4 kg, He fell from his father's arm onto a ceramic tile floor. Fall height as reported in the ER was 1.21m, which was revised to 1.28m during home visit. The infant sustained a nondisplace linear fracture through parietal bones, right longer and more distracted than left with a moderate sized right pareietal scalp haematoma.

RESULTS

In this section, we will discuss the following:

1. Variation of pulse width with drop height for adult PMHS tests.
2. Dependence of pulse width on contact surface for adult PMHS tests.
3. Goodness of estimated peak forces for adult PMHS tests.
4. Estimate of pulse width for neonate head drop tests.
5. Estimate of peak forces for test case collected in the ER.

Variation of pulse width with drop height for adult PMHS tests

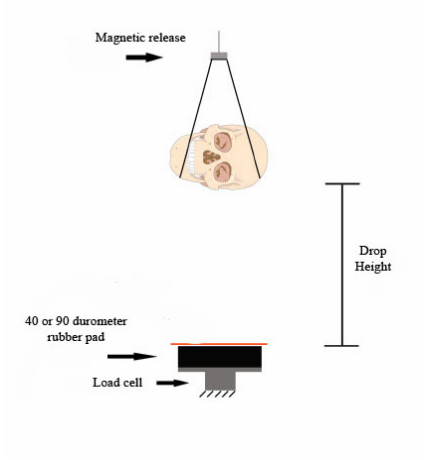

Figure 1: PMHS Head Drop Test Setup

Figure 1 illustrates the drop test setup. Figure 2 is a plot of vertical impact forces [F_z] recorded by the load cell on the platform under the rubber pad. In the drop tests under consideration, forces in the Y and X direction were negligible and only F_z was used in further calculations.

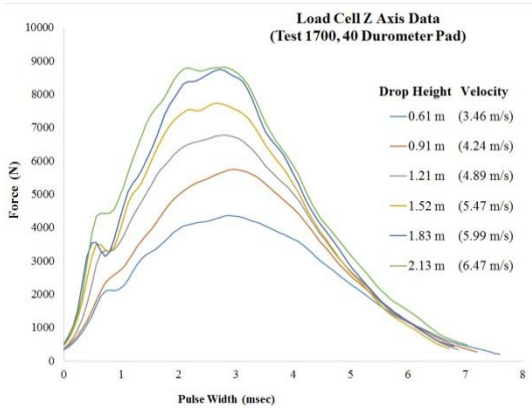

Figure 2. Vertical Force for various drop heights for one PMHS

Figure 2 shows the variation in F_z as a function of drop height, and therefore, velocity at contact with the rubber pad. It is seen that pulse shapes are similar and that pulse width is essentially the same for all drop tests. Note that the drop height has increased by a factor of 3.5 and so has the potential energy of the head. Higher contact

velocities resulted in higher forces. Data for these tests were obtained from drop tests of a disarticulated male head weighing 3.72kg onto a 61mm thick Shore durometer 40D rubber mat. Similar results were obtained in other tests.

Pulse widths for drop of a 4.48 kg [ID 1700] head onto Shore 40D durometer pad are tabulated in Table 2. It is seen that pulse width is more or less constant with a small standard deviation.

Table 2
Variation of pulse width with drop height.

Drop Ht, m	Contact Velocity, m/s	Pulse Width. ms
0.61	3.46	7.60
0.91	4.24	7.2
1.22	4.89	6.88
1.52	5.47	6.72
1.83	5.99	6.8
2.11	6.47	7.04
Mean		7.04
Standard Deviation		0.32

Table 2 indicates that there is very little variation in pulse width with increase in drop height.

Variation in pulse width between specimens for the same drop height is tabulated in Table 3. It indicates that even though the mass of the specimens vary, pulse width remains essentially the same.

Table 3.
Variation of pulse width with mass

ID	Pulse width, ms	Peak F_z, N	Mass, kg
1500	6.48	9103	4.37
1600	6.8	8020	3.52
1700	6.8	8759	3.72
1800	7.36	9352	4.48
1900	7.52	9277	4.52
Mean	6.99	8902	4.12
Standard Deviation	0.433	543	0.47

Dependence of pulse width on contact surface

Shore D stiffness can be used to calculate the Young's modulus of the rubber pad using the formula given below.

$\log (E) = 0.023(SD+50)-0.6403$ - 1

This formula indicates that the Young's modulus of the 40D and 90D pads, are, 4.18 MPa and 13.19 MPa respectively. The increase in stiffness of the pads is reflected in the higher F_z and shorter pulse widths seen in drops onto 90D pads as compared to drops onto 40D pads.

Difference in pulse width for 2 specimens of approximately the same mass when dropped from the same height onto to Shore 40D and 90D rubber pads is tabulated below. As expected, pulse width is narrower when the head is dropped onto a stiffer surface.

Table 4.
Pulse width and contact surface stiffness

Drop Ht, m	ID 2200, Mass 3.8kg		ID 1701, Mass 3.72 kg	
	Peak F_z, N	Pulse Width, ms	Peak F_z, N	Pulse Width, ms
0.61	4.24	7.2	4371	7.6
0.91	4.89	6.88	5351	7.2
1.21	5.47	6.72	6782	6.88

Goodness of estimates of peak F_z

Peak F_z for each drop test was estimated using the impulse-momentum theorem. It was assumed for the sake of simplicity that the force-time waveform had a tri-angular shape. With this assumption, impulse-momentum theorem can be written as:

$0.5*Fzpeak*pulse\ width = mass*contact\ vel$ -2

Knowing drop height, mass, and pulse width, peak F_z was calculated for each PMHS test. Measured and estimated peak F_z are tabulated in Table 5 for PMHS ID 1700 with a head mass of 3.72kg for a number of drop heights onto Shore 40D pad.

Table 5.
Comparison of estimated and measured peak forces

Drop Ht, m	Contact vel., m/s	Measured force, N	Estimated force, N	Diff, %
0.61	3.46	3654	3511	19
0.91	4.24	4476	4349	19
1.22	4.89	5168	5022	26
1.52	5.47	5778	5615	27
1.83	5.99	6330	6151	30
2.13	6.47	6837	6644	25

Similar results were obtained for all other PMHS drop tests for drops onto Shore 40D and 90D pads. Differences varied from about 1% to 30% and there was no seeming correlation of the differences to subject mass, contact velocity and stiffness of contacting surface.

This study assumed that the waveforms were tri-angular in shape and the area under the curve forms the left hand side of Equation 1. An examination of Fig.1 indicates that the area under the F-T curve will be higher than one obtained with a tri-angular approximation. Preliminary geometric experiments indicate that the area under the measured F_z – time curve might be approximately 20% higher than the value obtained with the tri-angular approximation. We propose to evaluate this more fully in future work.

Estimates peak F_z for case patient

Prange et al. [2004] conducted drop tests with 3 neonate heads dropped onto a steel plate from 15 and 30 cm heights. The authors indicate in their discussion that the average pulse duration was 18 ms. Using this information and anthropometric data collected in the ER, peak F_z for the case patient can be calculated using Formula 2. Relevant data are tabulated below.

Table 6.
Estimated contact force calculation

Weight, Kg	Est. Hd Wt, Kg	Est. Contact Vel, m/s	Est. Pulse width, ms	Est. Peak F_z
7.4	2.5	5	18	1392

The head mass can be used to estimate a head acceleration of 57G.

DISCUSSION AND CONCLUSIONS

This paper presents a simple, physics method to estimate impact loads on head in head drop tests. Estimates for forces exerted by the impacting surface on the adult PMHS heads have been compared with measured forces for 2 drop surfaces.

1. Maximum difference between estimated and measured head impact forces is in the range of 30% for head impacts into 90 and 40 Shore D pads with a majority of the estimates being in the 20% range.
2. Differences between measured and estimated forces does not depend on mass of the head or velocity at contact [or drop height].
3. This paper assumes that the head loading pulse is tri-angular in shape. In future work, we will consider the effect of pulse shape on the goodness of estimated force. Since most of the estimated forces are lower than measured forces by about 20%, it is likely that the estimates will be closer to the measured values if the area under the F-T curve was about 20% higher. In other words, the F-T pulse is not tri-angular in shape as assumed in this paper. Figure 1 illustrates that the Force-Time pulse is not triangular.
4. Our aim was to develop a simple robust method to estimate head impact loads that can be coded onto a spreadsheet and supplied to ER personnel. Assumption that the force-time waveform is tri-angular is justified by this requirement.
5. Proposed procedure underestimates impact forces. Therefore, any thresholds based on estimated forces are likely to be a conservative estimate.
6. The posture of the case patient will affect the peak contact loads and is unknown in this case.
7. Pulse duration for neonatal head drops may be different from that estimated for the case patient because of the interaction of body segments with the floor. However, it is reasonable to assume that since the child is so young, its reflexes may not be developed enough for it to take defensive action to prevent or modulate head injury.
8. Head mass of the case patient has been estimated to be 1/3 of the total weight. We propose to use geometry and scans in

future work to more correctly estimate the child's head mass.

REFERENCES

[1] Coats, B. 2007. "Mechanics of Head Impact in Infants". PhD Dissertation, UPenn.

[2] Irwin, A. and Mertz, H.J. 1997. "Biomechanical Basis for the CRABI and Hybrid III Child Dummies". SAE Paper 973317.

[3] Klinich, KD, Hulbert, G and Schneider, L. 2002. "Estimating Infant Head Injury Criteria and Impact Response Using Crash Reconstruction and Finite Element Modeling". Stapp Car Crash Journal, Vol. 46

[4] Melvin, J. 1995. "Injury Assessment Reference Values for the CRABI 6-Month Infant Dummy in a Rear-Facing Infant Restraint with Airbag Deployment." SAE Paper 950872.

[5] Prange, M.T, J.F. Luck, A. Dibb, C. Van Ee, R. Nightingale and B.S. Myers. 2004. "Mechanical properties and anthropometry of the human infant head" Stapp Car Crash Conference Journal, Vol. 48.

[6] Reece, RM and Sege, R. 2000. "Childhood head injuries: accidental or inflicted" Arch. Pediatr Adosesc Med 154(1):111-5.

[7] Roth, S, Raul, J-S, and Willinger, R. 2010. "Finite element modeling of paediatric head impact: Global validation against experimental data" Comp Methods and Prog in Biomedicine, 99, 25-33.

[8] Tarantino, C.A. et al. 1999. "Short vertical falls in infants" Pediatric Emer. Car 15, 5-8.

[9] Thibault, KL, and S.S. Margulies. 1999. "Age-Dependent material properties of the porcine cerebrum: effect on pediatric inertial head injury criteria. J Biomech. #31, 1119-1126.

[10] Wagner, CD. 2012. "Computational simulation of skull fracture patterns in pediatric subjects using a porcine model". PhD Dissertation, Wayne State University.

[11]Weber, W. 1985. "Zur biomechnischen Fragilität des säuglingsschädels" Z Rechtsmed 94. (93-101)

[12] Yoganandan, N, Zhang, J and Pintar, FA. 2004. "Force and Acceleration Corridors from Lateral Impacts". Traffic Injury Prevention, 5:368-373.

UPDATES OF THE LOWER EXTREMITY OF THOR-NT 50th FINITE ELEMENT DUMMY TO MOD-KIT SPECIFICATION

Neng Yue
Jaeho Shin
Matthew B. Panzer
Jeff Crandall
Center for Applied Biomechanics, University of Virginia
4040 Lewis and Clark Drive, Charlottesville, VA 22911

Dan Parent
National Highway Traffic Safety Administration, US DOT
1200 New Jersey Avenue SE, Washington, DC 20590

Paper Number 13-0328

ABSTRACT

This manuscript describes updates made to the lower extremity (knee-thigh (KT) and leg) of the THOR-NT 50th percentile finite element (FE) dummy, based on the geometry and mechanical characteristics of the THOR Mod Kit (MK) revision.

The geometry and mass of the FE KT region were updated to the same specifications as the THOR-MK design. The FE model knee-thigh compression and knee stretch responses were within the experimental test corridors and met the certification and biofidelity requirements of the THOR-MK. The model response from the knee pendulum impact test matched the dummy certification test data and was within the two first priority corridors of the knee slider certification requirements. An FE model of the molded shoe was developed using a three-dimensional scanning tool. The shoe model was validated using heel and ball-of-foot impact tests, and the simulated responses matched the experimental data. Three load cell modeling approaches were investigated and the locking joint method was the best approach considered for modeling load cells as rigid bodies.

Model updates to the THOR lower extremity and associated instrumentation were integrated into the THOR-NT FE dummy. The updated THOR-NT FE dummy model with the Mod Kit specifications in the lower extremity has the potential of providing improved responses in the frontal sled simulation and other applications.

INTRODUCTION

The Test Device for Human Occupant Restraint (THOR) anthropometric test device (ATD) was developed by National Highway Traffic Safety Administration (NHTSA) to improve upon the performance of the Hybrid III ATD (Haffner et al., 2001). Recently, Untaroiu et al. (2011) have performed the sensitivity analysis to assess the occupant injury risk using the THOR-NT finite element (FE) model undertaken by NHTSA. Choi et al., (2005) conducted the FE modeling effort of the THOR lower extremity and model verifications under different loading conditions and showed good agreement with the quasi-static and dynamic experimental results. Numerical simulations of a 40 % offset frontal crash with a small sedan and FE dummy models were performed and improved capabilities of the THOR lower extremity FE model were presented to assess the lower limb injury risk (Choi et al., 2005).

Recently, a hardware update to the THOR ATD (known as the THOR Mod-Kit) was developed to improve the durability, usability, and biofidelity of the THOR-NT ATD (Ridella and Parent, 2011). Included in this update were modifications to the lower extremity. The deformable length of the assembled femur was increased by 57% to match the biomechanical response of the human femur subjected to an axial impact at the intact knee (Rupp et al., 2003). The knee slider certification procedure and the newly-developed biofidelity requirement were adopted as the THOR-MK requirements to validate the knee slider biomechanical responses (Ridella and Parent, 2011; Balasabrarian et al., 2004). The softening of the rubber shear section of the knee slider and larger bumper stop were also implemented to improve the stiffness response. Finally, a one-piece molded shoe was developed to replace a military-specified (MIL-spec) shoe and a molded rubber foot, and improve the repeatability of the ATD response (Ridella and Parent, 2011).

Similarly, the FE model of the THOR-NT dummy was modified to incorporate the updates of the MK version of THOR. The objective of this paper is to describe the updates to the lower extremity of the THOR-NT FE dummy model and to validate the model based on the specifications for the THOR-MK ATD. Model validation was based on certification tests to the femoral shaft, knee slider, ankle joint, and molded shoe. The updated and validated lower extremity model of the THOR-MK was integrated into the whole THOR-NT FE model.

METHODS

Model Update and Validation of the Femoral Shaft

Modifications to the FE model were made to the new femur puck, guide system, load cell, and the interior rigid bar based on the updated geometry of the THOR-MK femoral shaft provided by NHTSA (Figure 1a). The densities of femoral guide system and thigh flesh were changed from 3.06 g/cm^3 to 2.63 g/cm^3 and from 0.44 g/cm^3 to 0.369 g/cm^3 respectively to meet the mass and inertial properties of the updated femur mechanical assembly (2.51 kg) and thigh flesh (1.05 kg). The geometry of the femoral puck (a compliant component to provide the compressive stiffness along the longitudinal direction of the femoral shaft) was revised to match the dimensions of the new puck design. Femoral puck response was based on the compression tests conducted by Humanetics Innovative Solutions, Inc during the development of the mod kit. Simulations of the femur puck compression consisted of a flat rigid plate compressing the femoral puck up to 15 mm at a rate of 1 m/s (Figure 1b). Compression force and displacement were recorded during the simulation, and parameters for a linear viscoelastic constitutive model were calibrated through a parametric study to match the experimental stiffness data.

The knee-thigh (KT) impact simulations were performed using the updated femur puck model to validate the computational response of femur shaft against the test data reported by Rupp et al. (2003). The femoral head was restraint from translational movement and the longitudinal axis of the femoral shaft was aligned with the impact direction. The knee had a flexion angle of 90°. The molded impactor (impactor with a molded face same as knee flesh) was controlled using a prescribed displacement time history and the impact force was recorded for comparison with the experimental test data (Figure 2).

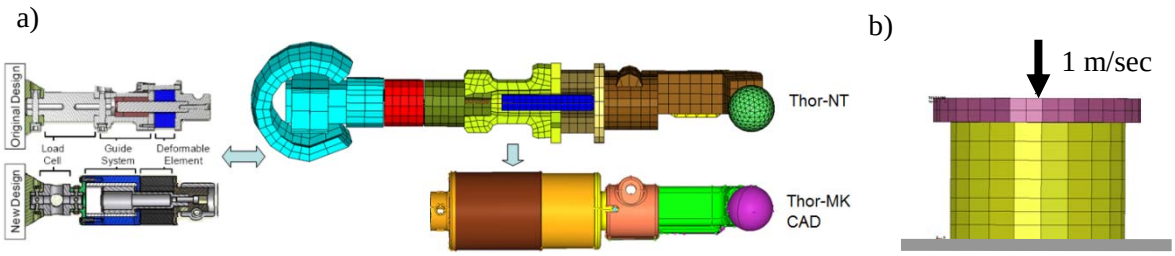

Figure 1. a) Femur shaft model update based on THOR-MK CAD data provided by NHTSA and b) compression test setup of THOR-MK femur puck model.

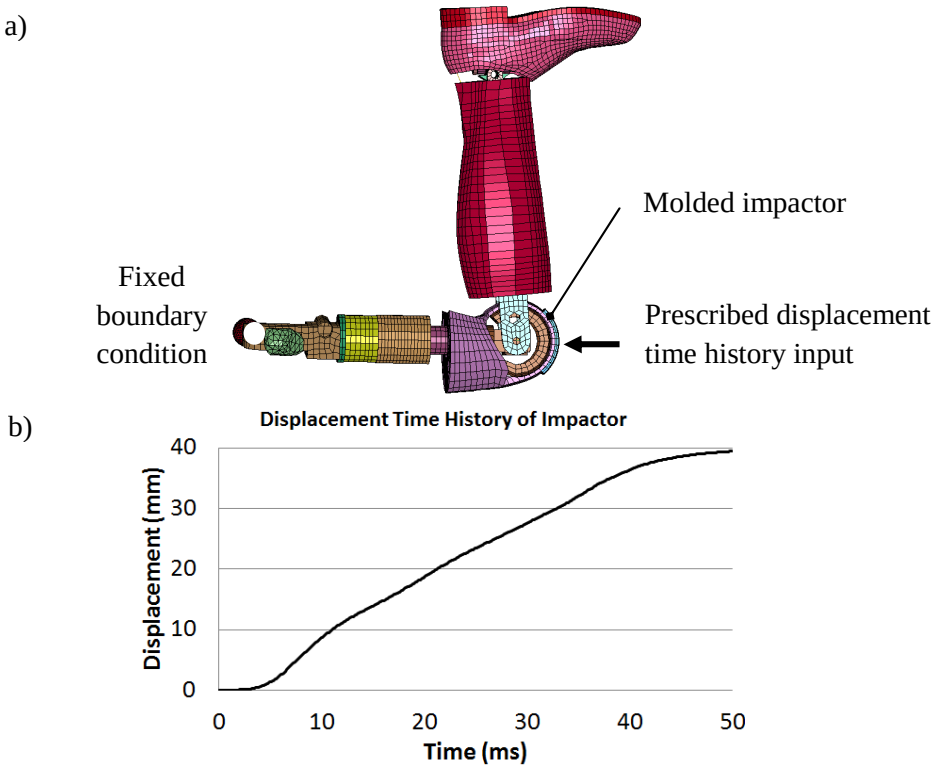

Figure 2. a) KT impact test setup (Rupp et al., 2003) for THOR-MK femur shaft FE validation and b) imposed displacement time history of impactor.

Model Update and Validation of the Knee Slider

The THOR-NT knee slider was modified to meet the newly-defined biomechanical response requirements for knee impact (Ridella and Parent, 2011). The previous THOR-NT FE dummy model did not include the knee slider and was limited in its ability to represent loading to the upper tibia. Therefore, a new FE knee slider model was integrated into the lower extremity model to simulate the response of the updated physical knee slider.

The knee slider consists of two articulating pieces connected by a sliding joint interface. The body of the knee slider (shown in green in Figure 3b) can rotate freely within the rigid knee assembly (shown in

orange in Figure 3b), while the outermost component of the slider (shown in blue in Figure 3b) can translate relative to the knee slider body. Translation between the outermost and knee slider body components is resisted by the shear deformation of the rubber connecting the two pieces. The outermost component is connected to the leg clevis, allowing the translational joint to rotate with the lower leg relative to the knee. Computationally, these joints were modeled as kinematic joints, with free rotation of the knee slider body relative to the knee and restrained translation of the outermost component of the slider relative to the knee slider body. The translational joint restraint was defined based on certification test data from tests on the physical ATD (Figure 11a). A stopper was modeled in front of the knee translational joint to prevent movement in the opposite direction.

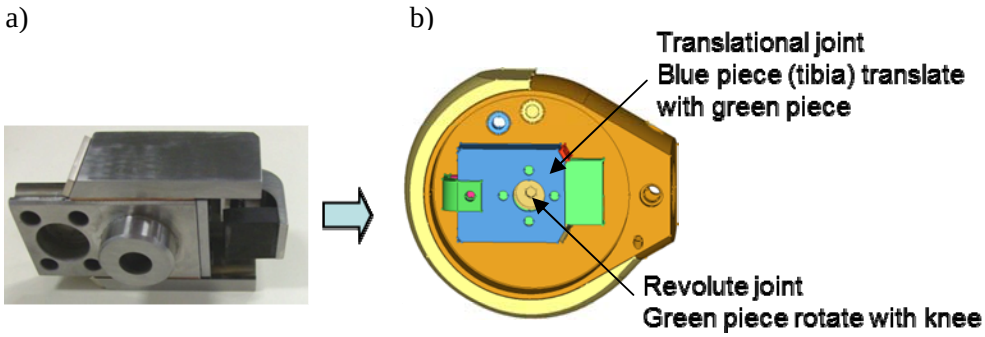

Figure 3. a) Physical knee slider of THOR-MK and b) three dimensional drawing of knee slider.

The stiffness response of the newly designed knee slider model was verified using the pendulum impact certification test on the physical THOR-MK ATD. This test mirrors the Hybrid III knee slider certification test, with a pendulum weight of 12 kg and impact surface diameter of 76.2 mm (Figure 4a). A 14.5 mm thick piece of low-density foam was placed between the knee clevis and the impactor. The knee clevis model was connected to the knee translational joints with two rigid beam models to ensure the force transmission to the knee rotational center. The knee translational joint was aligned with the impact direction and the pendulum model impacted the knee clevis with an initial velocity of 2.75 m/s. The displacement time history of the knee clevis and the reaction force at the femur shaft were recorded for response comparison with experimental data (Figure 4b).

Furthermore, the updated knee slider FE model was validated against the knee shear response of post mortem human subjects (PMHS) provided by Balasubramanian et al. (2004) for biofidelity check. The knee and leg model was set up with a 90° angle relative to the femur shaft and a constant velocity of 1.8 m/s along the anterior-posterior (A-P) direction was imposed to the tibia shaft. The reaction force at the femur shaft was processed using a SAE low-pass filter of 600 Hz (as done in the experimental test) to compare the model to the test data (Figure 4c).

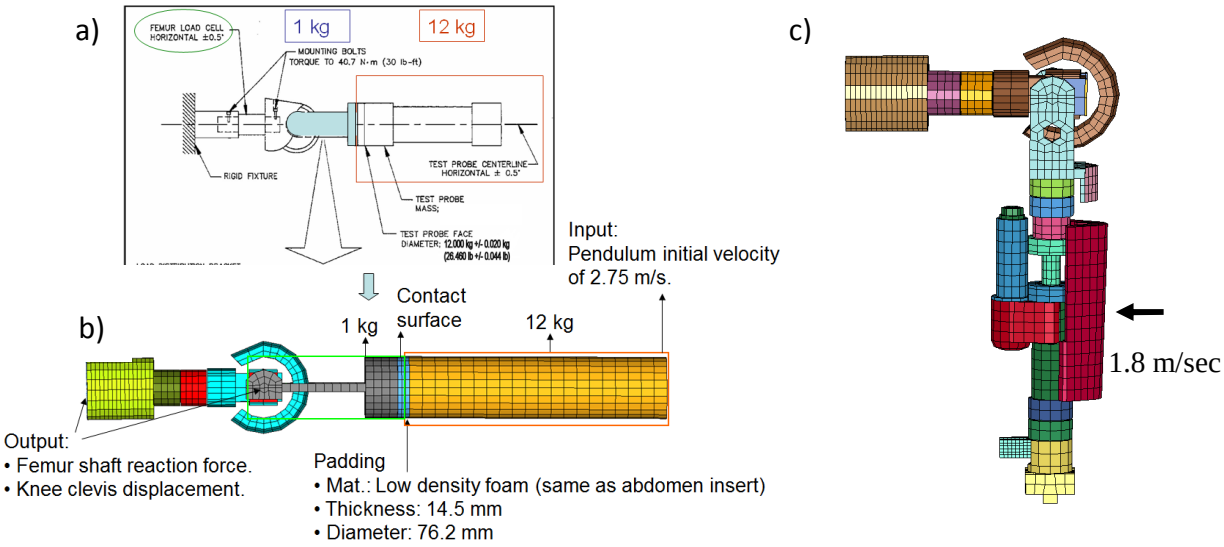

Figure 4. Certification validation setup of THOR-MK knee slider; a) physical certification test setup, b) FE simulation setup, and c) biofidelity validation setup based on the experiment performed by Balasubramanian et al. (2004).

Development of Molded Shoe Model

Because the three-dimensional geometry data for the THOR-MK molded shoe was unavailable, shoe geometry was obtained by scanning the surface of the molded shoe using a high speed laser scanning coordinate measurement machine (Focus 3D, FARO Technologies, Lake Mary, FL). The shoe was prepared by taping the outer surface for better scanning quality, and multiple scans were taken to ensure clean and complete surface data of the shoe. The FARO Scene software package was used to align all scans into a single point cloud (2.4 million points) and filter the data to eliminate outliers and noise (Figure 5).

A three-dimensional solid mesh of the molded shoe volume was generated in Hypermesh (Altair Engineering, Troy, MI) using the final point cloud dataset. The molded shoe FE model consisted of 2072 nodes and 1481 elements (Figure 5). Most elements in the shoe model (approximately 90%) were hexahedral elements with good mesh quality (minimum Jacobian of 0.57). The shoe material was modeled using a linear viscoelastic constitutive model with the material parameters calibrated using the dynamic heel impact test data (refer to next section). The total mass of the FE shoe model (1.38 kg) was close to the mass of the physical molded shoe (1.32 kg). The one-piece molded shoe FE model has replaced a military-specified (MIL-spec) shoe and a molded foot rubber of the THOR-NT FE model.

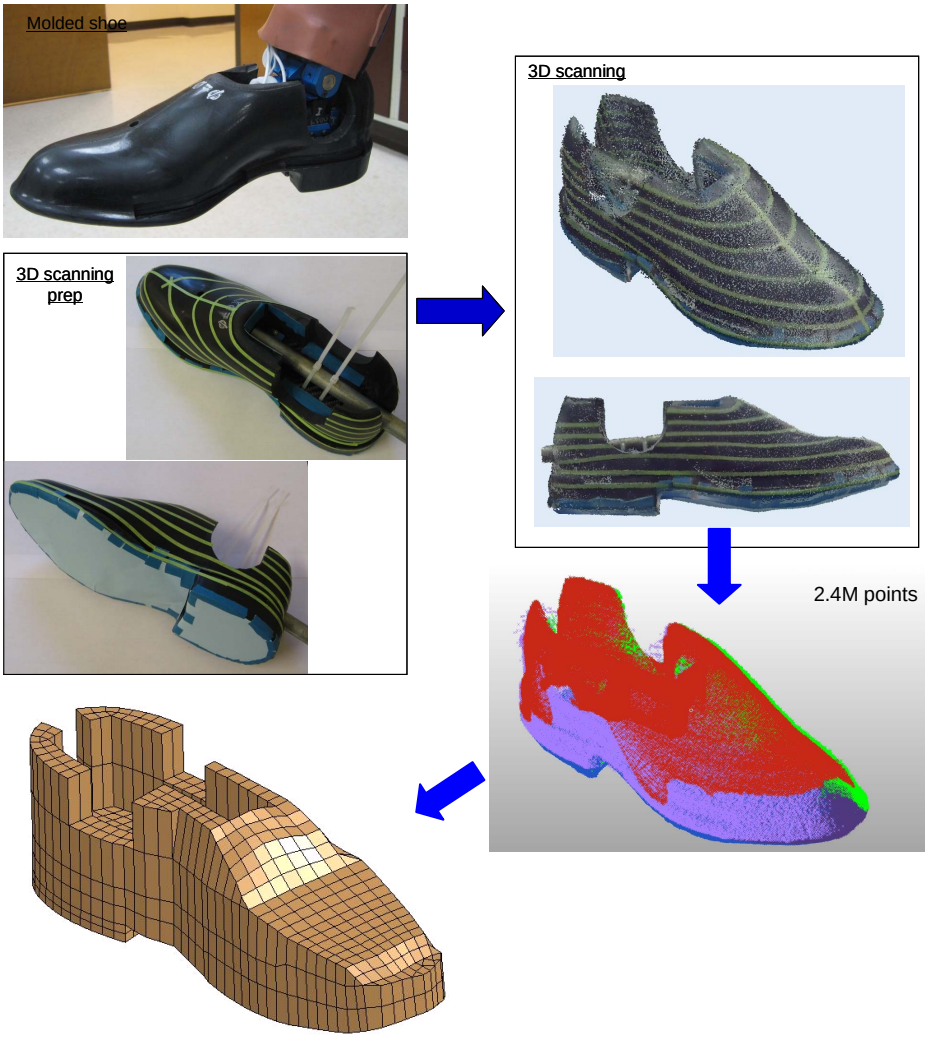

Figure 5. Development process of molded shoe FE model using the 3D laser scanning tool.

Heel and Ball-of-Foot Impact Tests and Simulations

The dynamic heel and ball-of-foot impact tests specified in the certification procedures for the THOR-LX were performed to validate the performance of the ankle and the compliant elements in the foot and tibia (NHTSA, 2004). There are two certification tests that specify impact with the 5.0 kg NHTSA dynamic impactor (cylinder shape with 63.5 mm diameter, NHTSA, 2004) to the molded foot: a heel impact at 4.0 m/s and a ball-of-foot impact at 5.0 m/s. These tests were conducted using the updated molded shoe of the THOR-MK hardware. The pendulum arm was mounted to a rigid shaft that pivoted on a low friction ball bearing. The proximal tibia was fixed rigidly with the Achilles cable and the toe pointing upward (0° flexion for heel impact and 15° plantar flexion for ball-of-foot impact, Figure 6). The impact point was aligned with the longitudinal axis of the tibia for heel impact tests, and 102.5 mm anterior of the dorsi-plantar joint for the ball-of-foot impact tests. The compressive force was measured in heel impact tests, while the force and moment time histories at the lower tibia load cell were recorded to calculate the ankle resistive moment and rotational displacement time histories were recorded. Six tests were run for each impact condition, and all data was processed using CFC600 filters.

To verify the updated THOR-MK molded shoe model, foot, and ankle response, heel and ball-of-foot impact simulations were performed. The heel impact simulations were performed with the FE shoe in the horizontal position, while the shoe FE model was rotated from 15° of plantarflexion to the neutral position and the Achilles cable was adjusted to match the ball-of-foot impact test configuration. The translational joint model and load cell model at the upper tibia were removed to mimic the certification test configuration (Figure 6). A linear viscoelastic material model was used for the molded shoe and the material parameters were iteratively tuned until the tibia force time history from the heel impact simulation reasonably represented those from the experiments.

The center of the impactor was aligned with the center of the dorsi-plantar joint for the heel impact simulation, and the impactor was set 102.5 mm anterior of the ankle joint for the ball-of-foot impact simulation. The impact speeds were 4 m/s (heel impact simulation) and 5 m/s (ball-of-foot impact simulation). The mass of the impactor was 5 kg in both simulations. The force time history of the lower tibia load cell was calculated in the heel impact simulation, while the ankle moment time history was determined in the ball-of-foot impact simulation.

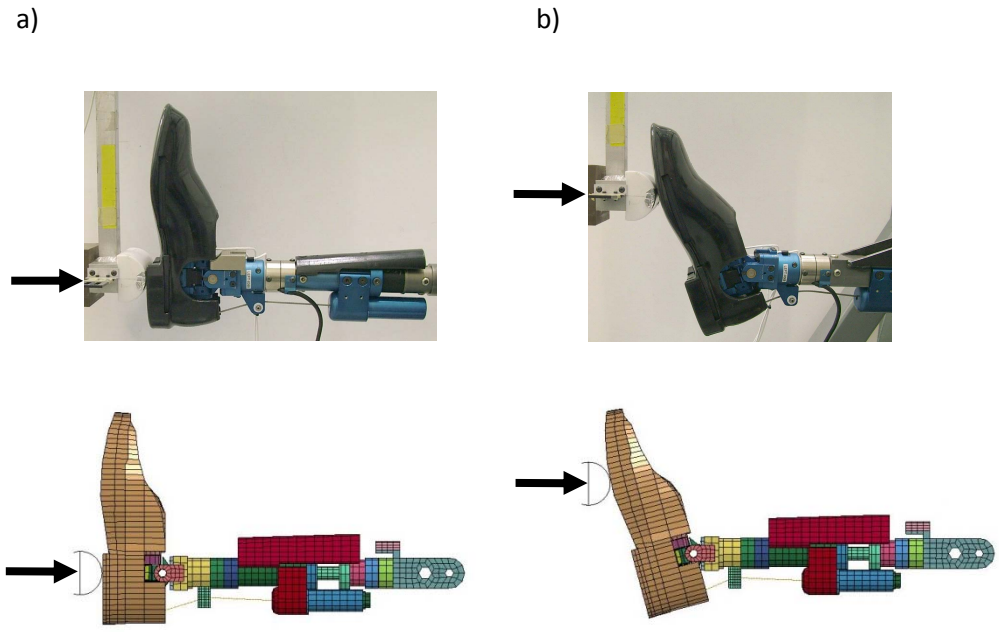

Figure 6. THOR-MK impact test and simulation setups of a) dynamic heel impact and b) dynamic ball-of-foot impact.

Investigation of Load Cell Modeling

To evaluate the force and moment output capabilities of the THOR-MK model, three modeling approaches were considered for modeling the load cells: the locking joint, the cross-section definition, and the beam element output. The simplified load cell was modeled as two pieces (Figure 7a), and the three different types of load cell models were setup connecting two pieces. The locking joint approach connected both pieces by fully constraining their relative motion, and forces were calculated as the

reaction force to satisfy this constraint. The beam element approach connected both pieces by a zero-length beam with high stiffness for all six degrees of freedom, and forces were calculated from the small deflections of the beam. The cross-section approach connected the pieces with shared nodes, and the sum of forces was calculated at this interface.

The local coordinate system was defined at the simplified load cell model to apply input loadings and calculate output data. A known force or moment was applied to one piece of the simplified load cell model and each model output was compared with the given input for modeling compatibilities. For the force input, the load (Figure 7b) was applied along the longitudinal axis of load cell defined as the z-axis of the local coordinate system, and a vertical load was applied along the x-axis of the local coordinate system to impose the y-axis moment. The calculated force and moment outputs were compared with the given inputs to check the modeling accuracy according to three different modeling concepts.

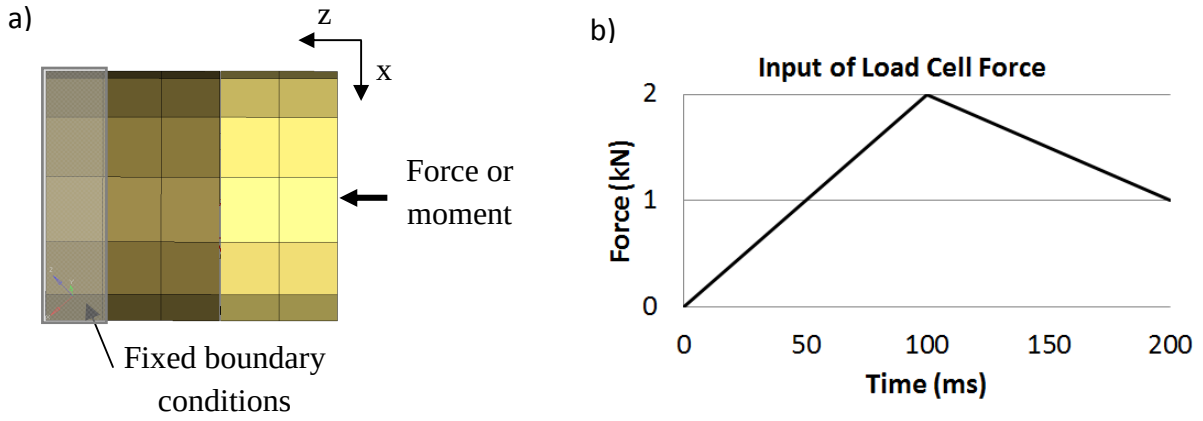

Figure 7. Conceptual modeling approach for load cell FE model; a) load cell components and simulation setup and b) input data of force time history for the model verification.

RESULTS

Model Update and Validation of the Femoral Shaft

The compression response for the updated femoral shaft model and femur puck (Figure 8a) was verified. The simulated compression force reached 4.8 kN at 15 mm of displacement, and matched the averaged experimental test data of 4.84 kN (Figure 8b). The viscoelastic material properties of the femoral puck calibrated to match the compression tests were applied to the updated FE model of the THOR-MK femoral puck (Table 1). Based on the viscoelastic constitutive models, the femur puck material in the THOR-MK design was softer than the puck material in the THOR-NT.

The stiffness characteristics of the THOR-MK femur model were validated using direct axial impact simulations. The model response was slightly stiffer than the experimental response of the physical THOR-MK (Figure 9). However, the THOR-MK femur model response showed good agreement with the biomechanical corridors developed by Rupp et al., (2003). The THOR-MK femur shaft showed a significantly decreased stiffness response than that of the previous THOR-NT model.

a)

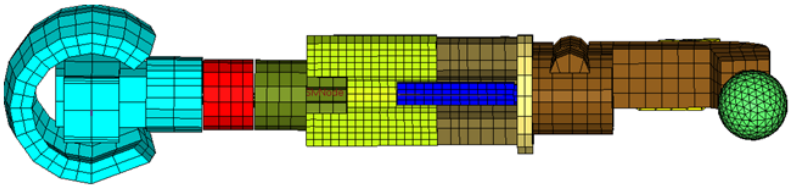

b)

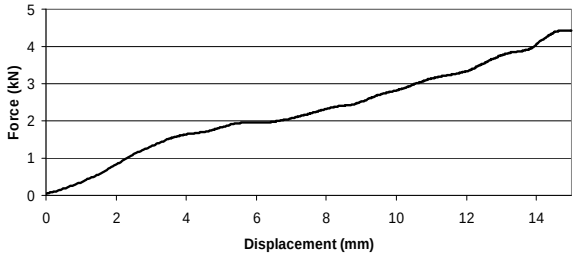

Figure 8. a) Updated femur shaft FE model based on THOR-MK CAD data provided by NHTSA and b) Force-displacement response of THOR-MK femoral puck model

Table 1. Material properties of femoral puck determined from iterative simulations

Material Model	*Viscoelastic*			
Properties	K (GPa)	G0 (GPa)	GI (GPa)	B (1/s)
Previous Values	7.0E-2	3.0E-3	1.0E-3	0.32
Updated Values	1.0E-2	2.5E-3	8.0E-4	0.32

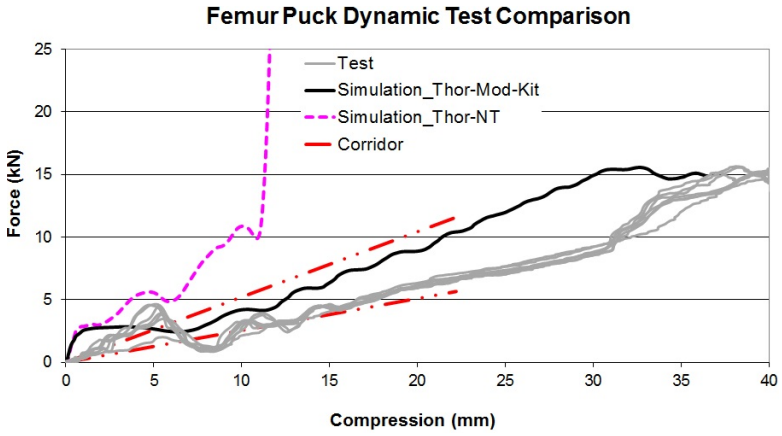

Figure 9. Comparison of force-displacement responses in KT impact among experiments and FE simulations.

Model Update and Validation of the Knee Slider

The force displacement response of the knee slider certification validation showed good agreement between the experiment and simulation (Figure 11a). For the knee slider biofidelity validation, the calculated stiffness response was in good agreement with the experimental results from Balasubramanian et al. (2004), although slightly less stiff (Figure 11b).

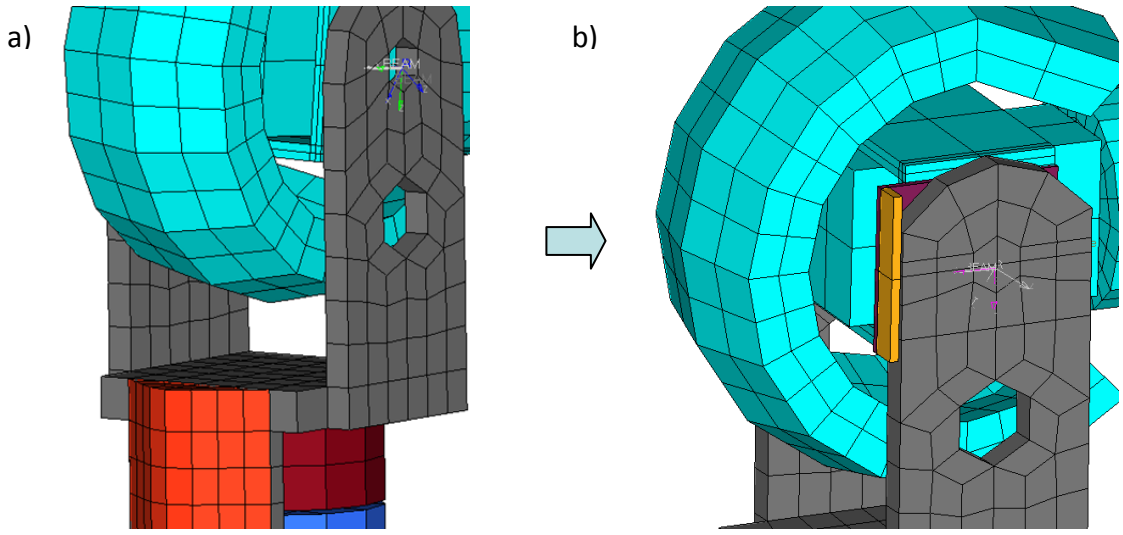

Figure 10. Knee slider designs of FE models, a) THOR-NT FE knee model and b) updated THOR-MK FE knee slider model.

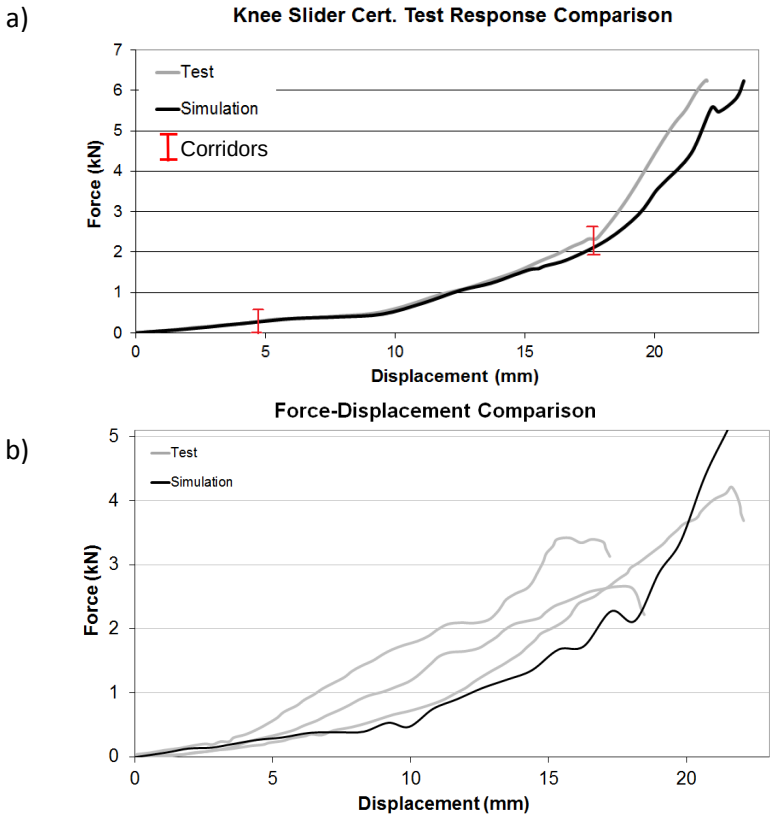

Figure 11. a) Force-displacement comparison of THOR-MK knee slider certification and b) force-displacement response of biofidelity validation according to Balasubramanian et al.'s experimental setup (2004).

Heel and Toe Impact Tests and Simulations

The heel and ball-of-foot impact tests specified in the certification procedures for the THOR-LX were conducted on the physical molded shoe and simulated using the updated THOR-MK lower extremity model. The six dynamic heel impact tests were showed good repeatability over the force time history of the impact (Figure 12). The peak compressive forces measured by the lower tibia load cell ranged between 2722 N and 2817 N at 10 ms. Subsequently, the corresponding heel impact simulation was performed and the force time history of lower tibia was calculated. The maximum peak force predicted by the model was 2769 N at 10 ms (Figure 12a). The results showed good correlation (the same level of peak forces at the same occurrence time) between the physical test and simulation responses, peak force levels, peak force occurrence times, and overall shape of the response curves.

The six dynamic ball-of-foot impact tests were conducted and used to validate the performance of the ankle and the compliant elements in the load path (molded shoe and ankle stopper) under dorsiflexion loading. The force and moment time histories at the lower tibia load cell were recorded. The peak ankle resistive moment calculated by the lower tibia force and moment were ranged between 44.0 Nm and 53.0 Nm, and the test responses showed good repeatability. Subsequently, the ball-of-foot impact simulation was performed using the same test configuration. The time history of ankle resistive moment was observed to have a peak of 49.9 Nm at 36 ms (Figure 12b). Good overall agreement was observed between the experimental and computational data for the loading phase, since the maximum moment calculated in the simulation is in the peak moment range obtained in the six tests.

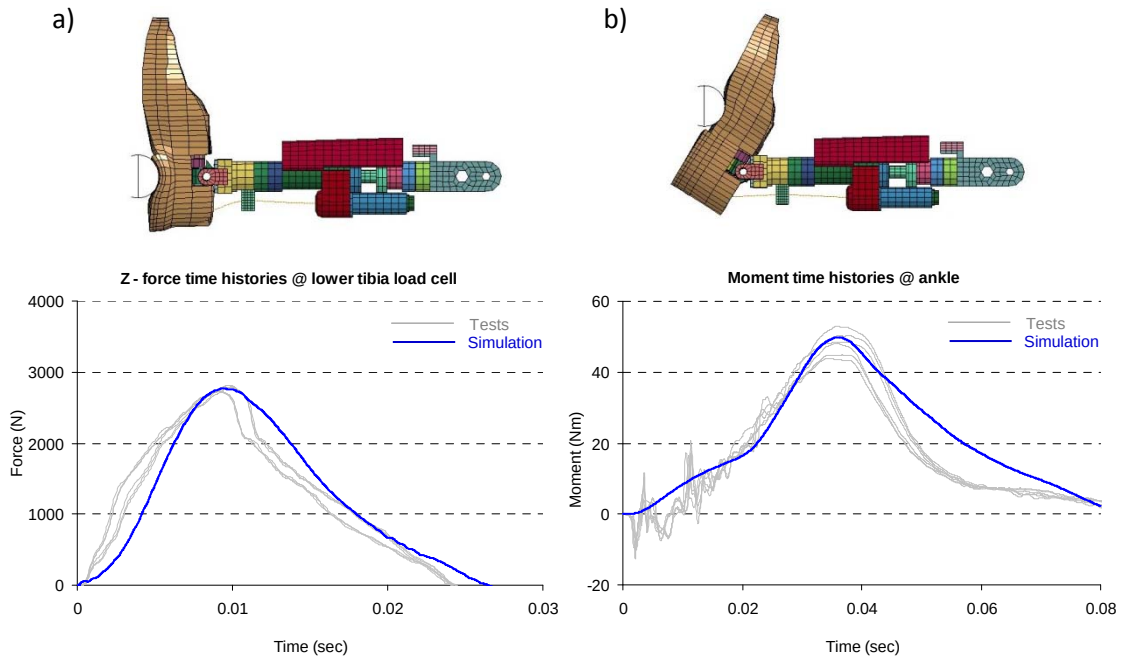

Figure 12. Comparison of FE model response under heel and ball impact loadings.

Investigation of Load Cell Modeling

Three types of load cell modeling methods were evaluated: the locking joint, the cross-section, and the beam element (Table 2). When representing axial force, all three approaches accurately measured the corresponding input profile. Thus, these three different load cell modeling concepts were all capable of recording forces in local coordinate systems. The moment output profiles of the locking joint and the cross-section were the same as the given input data, but the moment time histories of the beam element were not calculated. The locking joint and the cross section approaches are suitable for only rigid body and deformable body modeling, respectively (LSTC, 2007). Since the load cells in the THOR FE model were considered rigid for computational efficiency, the locking joint method was the recommended implementation strategy for load cells.

Table 2. Comparison of load cell modeling approaches

Approach	Force Output	Moment Output	Note
Locking joint	*Yes*	*Yes*	*For rigid body*
Cross-section	*Yes*	*Yes*	For deformable body
Beam element	*Yes*	No	

Integration into the THOR-NT Model

All FE model updates of the THOR-MK lower extremity, including the modified design of femur shaft, translational joint for knee slider, molded shoe, and foot modification, were incorporated into the whole dummy FE model (Figure 13).

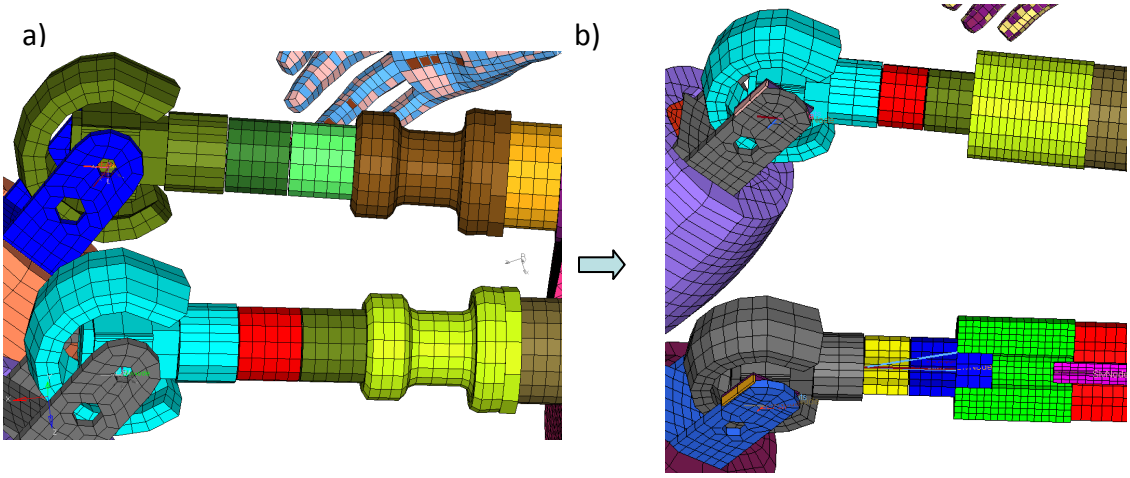

Figure 13. THOR-MK updates in the femur shaft and knee slider regions; a) THOR-NT knee-thigh region and b) THOR-MK knee-thigh region.

DISCUSSION

THOR lower extremity FE model consists of approximately 17000 nodes and 12000 elements based on the three-dimensional drawings of the physical hardware. While most parts in the actual THOR dummy were represented, some parts were simplified to increase the model stability and reduce the total calculation time during FE simulations. While the skin of the THOR lower extremity was modeled as an elastic material, the femur puck, tibia compliance bushing and foot padding were represented by linear viscoelastic materials. The deformable seatbelt model was used for the Achilles cable, and components made of steel or aluminum were modeled as rigid bodies for FE simulation efficiency.

One limitation of the current THOR model is that only the lower extremity part of the current dummy model was updated to the THOR-MK version. The hardware discrepancy in other body regions might introduce the different response when comparing the current updated THOR-NT FE model with the physical THOR-MK dummy. The head and neck, shoulder, and pelvis of the THOR-NT FE model will be updated in the near future to match the MK specifications. Once all body regions are assembled to the global model, several full body validations will be conducted to assess its responses against the test data. The THOR-MK model will have the potential of better predicting the driver kinematics and injury responses than its predecessors under various applications, such as the small overlap oblique impact scenarios.

The molded shoe FE model of THOR-MK was developed using the three dimensional scanning tool in this study. The three-dimensional geometry data of the molded shoe was obtained by a high speed laser scanning coordinate measurement tool. While millions of points (x, y, and z coordinates) were collected covering the surface of the molded shoe, the point cloud data should be carefully checked and filtered to remove some noisy data. The point data was transferred to the pre-processing software for constructing FE models. Finally, this procedure from the three dimensional scanning data to the FE model was better for accurately modeling the complex geometry.

CONCLUSIONS

The lower extremity of THOR-NT FE dummy was updated to the THOR-MK specification by improving the certification and biofidelity capabilities of the femoral shaft, including the knee slider (translational joint), updating the load cell modeling approach, and developing the molded shoe model. The heel and ball-of-foot impact simulations were performed with the developed molded shoe FE model. The calculated responses of both impact simulations showed good agreement with the experimental responses. Additional updates to the other body regions of the current dummy model are necessary to better understand the dummy response during vehicle crash tests and develop advanced restraint systems.

ACKNOWLEDGEMENTS The authors acknowledge the support and guidance of the National Highway Traffic Safety Administration (NHTSA), U S Department of Transportation. This study was supported by DOT NHTSA Cooperative Agreement DTNH22-09-H-00247. All findings and views reported in this manuscript are based on the opinions of the authors and do not necessarily represent the consensus or views of the funding organization.

REFERENCES

Balasubramanian, S., Beillas, P., Belwadi, A. et al. (2004) Below Knee Impact Responses using Cadaveric Specimens, Stapp Car Crash Journal, Vol. 48.

Choi, H. Y., Shin, J. Y., Lee, I., Ahn, C. N., Bae, H. I. (2005) Finite Element Modeling of THOR-LX and its Application, SAE Paper No. 05-0125.

Haffner, M., Rangarajan, N., Artis, M. et al. (2001) Foundations and Elements of the NHTSA THOR Alpha ATD Design, 17th ESV Conference, Paper No. 458.

LSTC (2007) LS-DYNA Keyword User's Manual, Version 971.

NHTSA VRTC (2004) Certification Procedure for the THOR-LX/Hybrid III Retrofit Version 3.2

Ridella, S., Parent, D. (2011) Modifications To Improve The Durability, Usability And Biofidelity of The THOR-NT Dummy, Proceedings of the 22th International Technical Conference on the Enhanced Safety on Vehicles, NHTSA, Washington D.C.

Rupp, J. D., Reed, M. P., Madura, N. H. et al. (2003) Comparison of Knee/Femur Force-deflection Response of the THOR-NT, Hybrid III, and Human Cadaver to Dynamic Frontal-impact Knee Loading, Proceedings of the 18th International Technical Conference on the Enhanced Safety on Vehicles, NHTSA, Washington D.C.

Untaroiu, C., Lu, Y-C. (2011) A Simulation-Based Calibration and Sensitivity Analysis of a Finite Element Model of THOR Head-Neck Complex, SAE Paper No. 2011-01-1123.

SEAT OPTIMISATION CONSIDERING REDUCTION OF NECK INJURIES FOR FEMALE AND MALE OCCUPANTS – APPLICATIONS OF THE EVARID MODEL AND A LOADING DEVICE REPRESENTING A 50th PERCENTILE FEMALE

Paul Lemmen, Amit Gupta, Apoorva Lakshminarayana
Humanetics Innovative Solutions
Germany
Anna Carlsson, Mats Svensson
Chalmers University of Technology
Sweden
Kai-Uwe Schmitt
AGU Zurich
Switzerland
Ines Levallois
Faurecia
France
Astrid Linder
The Swedish National Road and Transport Research Institute
Sweden
Ernst Tomasch
Graz University of Technology
Austria
Paper Number 13-0220

ABSTRACT

Neck injury due to low severity vehicle crashes is of worldwide concern and the injury risk is greater for females than males. However, whiplash protection systems have shown to be more beneficial for males than females. Hence there is a need for improved tools to address female protection.
One objective of the European 7th Framework, project ADSEAT was to develop a finite element model of a rear impact dummy representing females for application in seat optimization studies along with the BioRID II. In support of this injury risks for females were studied revealing target size for the dummy model. Related anthropometric data were derived from literature and dynamic volunteer tests comprising females performed to set biofidelity targets. On this basis a finite element model representing females was developed and relevant injury criteria and thresholds identified. For the latter use was made of a prototype loading device consisting of a modified BioRID dummy that better matches the female anthropometry.
This paper article documents the development of the female whiplash dummy model called EvaRID (Eva female, RID – Rear Impact Dummy) and its application to a series of production seats. The loading device BioRID50F and initial test results are also presented herein.

INTRODUCTION

Motivation

Whiplash Associated Disorders (WAD), or 'whiplash injuries', sustained in vehicle crashes is a worldwide concern. In Sweden, such injuries account for about 70% of all injuries leading to disability due to vehicle crashes [1]. The majority of those experiencing initial neck symptoms following a car crash recover within a few weeks or months after the crash as reported by The Whiplash Commission [2]. However, 5 to 10% experience varying degrees of permanent disabilities [2] to [4]. Whiplash injuries may occur at relatively low velocity changes, typically less than 25 km/h [5], [6], and in impacts from all directions. Rear impacts occur most frequently out of all recorded impacts in accident statistics [7].
It is well established that the whiplash injury risk is higher for females than for males, even in similar crash conditions [8] to [18]. These studies concluded that the female injury risk was 1.5 to 3 times higher than the male injury risk. Females and males have different anthropometry and mass distribution, which may influence the interaction between the upper body

and the seatback/head restraint, and thus the injury risk. For example, the deflection of the seat frame, seatback padding and springs may depend on the mass and/or the centre of mass of the upper body with respect to the lever about the seatback hinge. The deflection of the structures of the seatback affects the plastic deformation, energy absorption and the dynamic head-to-head restraint distance, as well as the rebound of the torso [19] to [21]. The motion of the head relative to the head restraint may be affected by seated height in relation to the head restraint geometry. It has been reported that females have a somewhat different dynamic response in rear volunteer tests, such as a higher head forward acceleration, a higher (or similar) T1 forward acceleration, a lesser (or similar) Neck Injury Criterion (NIC) value and a more pronounced rebound than males [20] to [31].

Crash test dummies are used when developing and evaluating occupant protection performance of a vehicle. For whiplash injury risk assessment the BioRID II dummy is being used which represents a 50th percentile male. However, the dummy size corresponds to a ~90th–95th percentile female with regards to stature and mass [32], resulting in females not being well represented by this tool. Consequently, the current seats and whiplash protection systems are primarily adapted to the 50th percentile male with little or no consideration of female properties. Existing whiplash protection concepts are approx. 30% more effective for males than for females according to insurance claims records [33]. The difference between protection for females and males has effectively increased although the overall whiplash injury risk has decreased in rear impacts. Further investigations into these differences and understanding of the reason behind them are needed in order to achieve better protection for both genders.

Objectives

In view of the above, the ADSEAT (Adaptive Seat to Reduce Neck Injuries for Female and Male Occupants) project was initiated. The overall objective of ADSEAT is to provide guidance on the protective performance evaluation of vehicle seats, aiming to reduce the incidence of whiplash injuries. The work focussed on evaluating the protective performance of seats for female and male occupants. Hence the development of an average female size finite element (FE) crash dummy model was undertaken. The new research tool, EvaRID, is intended as a complement to the BioRID II dummy when evaluating enhanced whiplash protection systems.

Approach

Figure 1 depicts the approach used to develop the EvaRID model. As a first step the size for the model was identified. Injury statistics were extracted from insurance databases revealing that a 50th percentile female dummy would correlate in size to the females most frequently suffering whiplash injury. Anthropometric data were then collected to define the geometry and mass. Based on these data a BioRID II dummy model was scaled to result in the EvaRID model that represents females. Extensive validations were made at volunteer level. Corridors from two datasets were used in an interactive procedure to fine tune and validate the model response.

Injury criteria and thresholds were derived. Amongst others an analysis of insurance data comparing risk for females with that of males was made to give thresholds related to NIC. In addition a new mechanical loading device called BioRID50F, crudely representing the anthropometry of a 50th percentile female, was developed [34] and applied in sled tests. Results for BioRID50F and BioRID II were compared for a range of seats to provide confidence in the thresholds established.

Finally the EvaRID model was applied to a range of seats under various loading conditions. Predictive injury outcomes of EvaRID were compared with those for BioRID II.

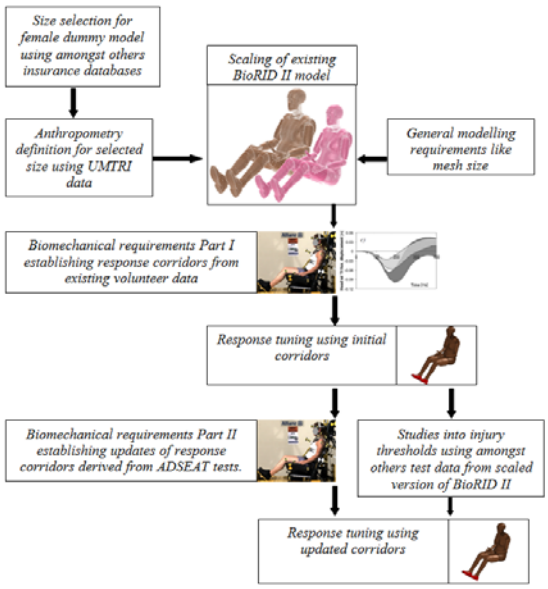

Figure 1 –EvaRID development process.

SIZE SELECTION FOR EvaRID MODEL

Within the scope of the ADSEAT project, several sources were evaluated to establish the anthropometry of females sustaining WAD most frequently [35]. An extensive literature review, searching for risk factors and injury criteria for males and females in published literature was performed. The review revealed that, until now, anthropometric measurements like body height, weight and head to neck ratio have not been established as a risk factor. Older studies associate a taller stature with an increased WAD risk [36] and [37], although it should be noted that those studies include seats not equipped with whiplash protection systems and conditions have changed since protection systems were introduced in vehicles. For instance, the mid- and long-term risk of WAD tend to decrease for increasing statures in vehicles equipped with the SAHR system [38], while in vehicles equipped with the WhiPS system stature does not appear to influence the risk of sustaining WAD [39].

A review on injury criteria showed that there are no gender specific injury criteria. Furthermore, no validated methods to adequately scale proposed threshold values were found. Nonetheless real-world data analysis reveals existing whiplash protection concepts to be more effective for males than for females, at a 45% risk reduction in permanent medical impairment for females and 60% for males [33]. For this reason insurance data were used to establish the size for the female model. Records of females who have sustained whiplash injuries in rear impacts were extracted from the AGU Zurich database, Switzerland (N=2,146), and the Folksam database, Sweden (N=1,610). Stature and mass distributions of the injured females are shown in Figure 2. The injured females in the AGU Zurich database had an average stature/mass of 165.3 cm/65.2 kg, which is close to the average size of the female population in Switzerland, 164.7 cm/63.4 kg (verbal confirmation by Swiss Statistical Office). Correspondingly, the average stature/mass of the injured females in the Folksam database was 165.3 cm/65.2 kg for, which correlate well with the average size of the female population in Sweden, 165.9 cm/65.9 kg [40]. Thus, it was considered that the 50th percentile female dummy would correlate best in size to the females that are most frequently injured in rear impacts. A comparison of these measures with data of the general female population of other European countries indicates that the weight and height found for the females that most frequently sustain WAD corresponds quite well with the average anthropometry among European countries; that is 165 cm and 66 kg (Table 1).

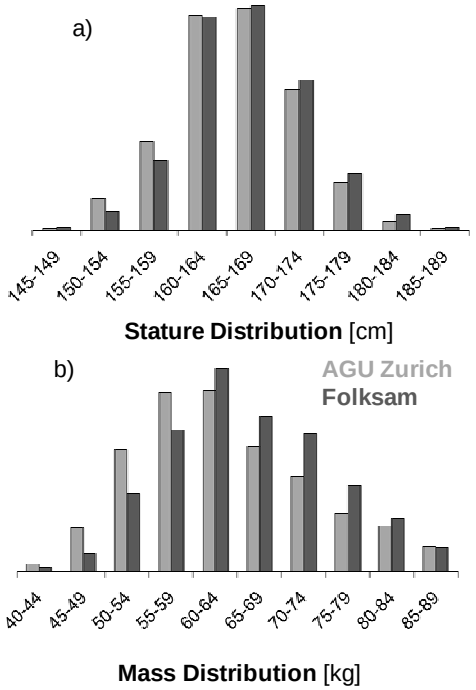

Figure 2 – Stature and mass distributions of whiplash injured female occupants in Sweden (Folksam database) and Switzerland (AGU Zurich database).

Table 1 – "Average" female anthropometry of the general population in different European countries

Country	Height [cm]	Weight [kg]	Age [years]
Austria [e, g]	167	67	43.2
Czech Rep. [e, f]	167.3	-	41.9
Germany [c, e]	165	67.5	45.2
Finland [e, f, h]	164.7	69-83	43.7
France [b, e, g]	161.9	62.4	40.9
Italy [e, g]	162	-	44.8
Netherlands [d, e]	166.8	68.1	41.2
Spain [e, f]	161	-	42.5
Sweden [e, i]	166.8	64.7	42.6
Switzerland [a, e]	164	49-67	42
UK [e, h]	161.6	67	41.3
Average	164.6	66.3	42.5

[a] www.statistik-bs.ch/kennzahlen/integration/A/a2
[b] www.insee.fr/fr/ffc/docs_ffc/es361d.pdf
[c] www.wissen.de/wde/generator
[d] dined.io.tudelft.nl/en,dined2004,304
[e] www.cia.gov/library/publications/the-world-factbook
[f] www.disabled-world.com/artman/publish/height-chart.shtml
[g] www.imas.at/content
[h] psychology.wikia.com/wiki/Body_weight
[i] www.nordstjernan.com/news/sweden/776/

In order to make a decision on the size to be used including a reference to a dataset that includes all required anthropometry information for defining in detail the dimensions of the female dummy model reference is made to assumptions made when defining the WorldSID dummy. For defining the anthropometry of that dummy it was concluded [41] that the size of a world-harmonized 50th percentile adult male would correspond well with the size of the 50th percentile adult male as defined by UMTRI [42] to [44]. For this reason it was regarded appropriate to assume the same for the 50th percentile adult female. Thus, it was decided to base the EvaRID model on the anthropometric measures of the 50th percentile female from the UMTRI study with a stature of 161.8 cm and a mass of 62.3 kg. Table 2 compares main dimensions with those from other dummies.

ANTHROPOMETRY SPECIFICATIONS

Having established the stature, mass and seated height of the EvaRID model, the next step was to specify the dimension and mass of different body segments and the distance between joints for the 50th percentile female. The UMTRI study [42] to [44] described in detail how the anthropometry and properties were specified for the 5th percentile female, as well as for the 50th and 95th percentile male crash test dummies. The same method was used in this study, if appropriate, when establishing the anthropometry of EvaRID. However, the actual data had to be found elsewhere since the UMTRI study did not contain relevant information for the 50th percentile female.

The anthropometric data for the 50th percentile female was mainly collected from the studies described by Diffrient et al. [45] and Young et al. [46]. In addition, anthropometric data extracted from the ergonomic software programmes GEBOD [47] and RAMSIS [48] was used to validate the collected data. Product Information from Humanetics (previously FTSS) was used to collect information on the BioRID II hardware dummy for direct comparison of anthropometric data. Finally, parts of the 50th percentile male data from McConville et al. [49] were used for comparative purposes.

In [46] the 50th percentile female stature was 161.2 cm and the mass 63.9 kg; i.e., 0.4% shorter and 2.6% heavier than the 50th female values in Table 2. In [45] the 50th percentile female stature was 161.5 cm and the mass 65.8 kg; i.e., 0.2% shorter and 5.6% heavier than values in Table 2. Due to the small differences in stature, scaling was not made to the length dimensions in [45] and [46]. As mass differences were found to be greater, the depth and width dimensions or circumferences were scaled according:

- Young et al. (1983) [46]: 1% scaling
- Diffrient et al. (1974) [45]: 2% scaling

The EvaRID model was developed by scaling an existing BioRID II model from DYNAmore GmbH [52]. As described in the next section, this was done segment by segment according to the segments defined in [46]. The distances between joints were taken from [45] and summarised in Figure 3. Regression equations from [46] were used to compute the segment volumes [50].

Table 2 – Stature, mass and seated height of dummy family [42].

%-ile	Sex	Stature [cm]	Mass [kg]	Seated Height [cm]
5th	Female	151.1	47.3	78.1
50th	**Female**	**161.8**	**62.3**	**84.4**
50th	Male	175.3	77.3	90.1
95th	Male	186.9	102.3	96.6

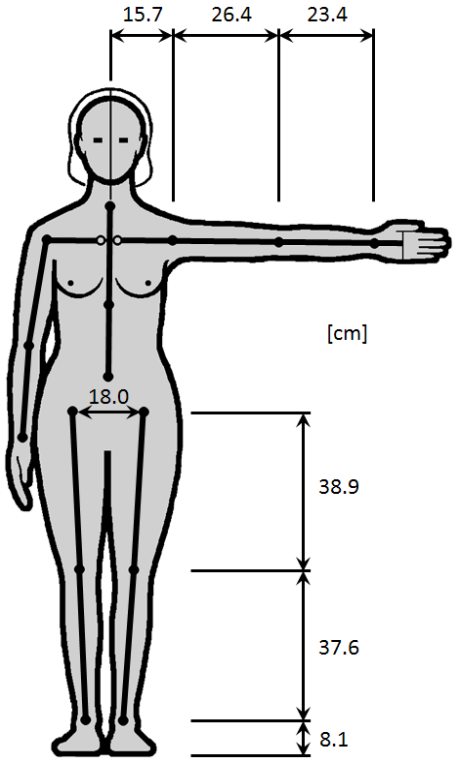

Figure 3 – Distances between joints of EvaRID [45].

Table 3 – Mass, mass distribution (in percentage of the total mass), and Mass Ratio (MR) (M_{EvaRID}/M_{BioRID}) of BioRID II and EvaRID.

Body Part	EvaRID		BioRID		MR
	Mass [kg]	% of total	Mass [kg]	% of total	Mass Ratio
Head	3.58	5.7	4.54	5.8	0.789
Upper Torso[1)]	19.58	31.4	26.61	34.0	0.736
Pelvis[2)]	15.84	25.4	15.80	20.2	1.003
Upper Arm	1.40	2.2	2.02	2.6	0.691
Lower Arm[3)]	1.16	1.9	2.23	2.9	0.518
Upper Leg[4)]	5.67	9.1	5.99	7.7	0.947
Lower Leg[5)]	3.43	5.5	5.44	7.0	0.631
Total	**62.30**	**100**	**78.24**	**100**	**-**

1) The upper torso consists of the thorax, abdomen, spine and neck.
2) Flaps included.
3) Hand included.
4) Flap excluded.
5) Foot included.

The mass of each body segment was estimated based on its volume, assuming constant density of the body. The resulting masses (absolute and relative compared to overall mass) and the Mass Ratio (MR) of body parts for the EvaRID and BioRID II dummy models are provided in Table 3. Slight differences in mass distribution can be seen between the female EvaRID and the male BioRID; males having somewhat more mass in the torso region while the mass is greater in the pelvic region of females. Relevant anthropometry data in terms of segment volumes and main dimensions are provided in [50].

EvaRID MODEL DEVELOPMENT

When developing the EvaRID model by scaling the BioRID II model, the goal was to make sure that mass, inertia and length data of each body segment matched the anthropometric data for the 50th percentile female as closely as possible. To meet anthropometric requirements in terms of mass and dimension, firstly the longitudinal dimensions and mass were scaled according to equations (1) and (2) below. Breadth (width) and depth dimensions for the different EvaRID body parts were established based on the most appropriate scaling method for each body segment. For the purposes of this article, SFL is the Longitudinal Scale Factor, SFB the Breadth Scale Factor, and SFD the Depth Scale Factor.

Extremities – It was assumed that SFB and SFD for the extremities / limbs are equal. SFB / SFD then follow as the square root of Mass Ratio over Scale Factor Length (volumetric relationship), see Table 4.

Head - For the head, all data for breadth and width scaling directions were available in the anthropometry specifications. Due to the head´s importance in terms of loading to the neck it was decided to apply direct scaling in all directions to meet all the dimensional requirements.

Neck – Adequate sources were not found when collecting input data for the anthropometry defining the skeleton. Of particular relevance are the spine and neck, and due to the lack of data it was decided that EvaRID would maintain the same spine and back profile as in BioRID II. This was achieved by keeping the length and depth scaling factors, *SFL* and *SFD*, identical for both the neck and torso. Furthermore, it was assumed that breadth scaling factors SFB_{neck} and SFB_{torso} are identical, concluded by comparing the shoulder joint distance of EvaRID to the shoulder joint distance of BioRID.

Torso - The upper torso was defined as the torso without the pelvis, running from the cervical to the iliac crest. The mass of the upper torso was derived by subtracting the mass of the pelvis from the mass of the torso. The breadth scale factor, SFB, was obtained by comparing the distance between shoulder joints in the female data (31.50 cm) and the value for the BioRID II (34.60 cm). *SFD* was then calculated according to the equation in Table 4.
The outer shape of the male and female torso and pelvis segment body parts differ significantly. Breasts would be added to the female dummy and the shoulder/ waist ratio for both genders were quite different. Therefore, further refinements were made to the uniform scaling applying *SFL*, *SFB* and *SFD*. Using anthropometric data from Diffrient et al. [45] and Young et al. [46] the waist breadth was set at 310.5 mm, bust 288 mm; 10th rib 257 mm; buttocks 373 mm; and bust point distance 180 mm. Information on circumferences from these data sources was also used to further shape the geometry.

Pelvis - Although the outer shapes are different for the pelvis, no significant difference between the main dimensions of the 50th percentile female and the 50th percentile male pelvis were found in the anthropometric studies described in [46] and [49]. Furthermore, the distance between the hip joints was similar for the 50th percentile female and the BioRID II. The pelvis mass was also found to be similar for the 50th percentile male (15.84 kg) and the 50th percentile female (15.80 kg). Consequently, the shape of this body part was the only one adjusted to match

Table 4 – SFB and SFD equations for body parts

Part	SFB	SFD
Head	$\frac{\text{Head Breadth}_{\text{EvaRID}}}{\text{Head Breadth}_{\text{BioRID}}}$	$\frac{\text{Head Depth}_{\text{EvaRID}}}{\text{Head Depth}_{\text{BioRID}}}$
Neck	$= \text{SFB}_{\text{upper torso}}$	$= \text{SFL}_{\text{neck}}$
Upper Torso	$\frac{\text{Shoulder Breadth}_{\text{EvaRID}}}{\text{Shoulder Breadth}_{\text{BioRID}}}$	$\frac{\text{MR}_{\text{upper torso}}}{(\text{SFL}\times\text{SFB})_{\text{upper torso}}}$
Pelvis	1	$\frac{\text{MR}_{\text{pelvis}}}{(\text{SFL}\times\text{SFB})_{\text{pelvis}}}$
Extremities	$\sqrt{\frac{\text{MR}_{\text{limb}}}{\text{SFL}_{\text{limb}}}}$	$\sqrt{\frac{\text{MR}_{\text{limb}}}{\text{SFL}_{\text{limb}}}}$

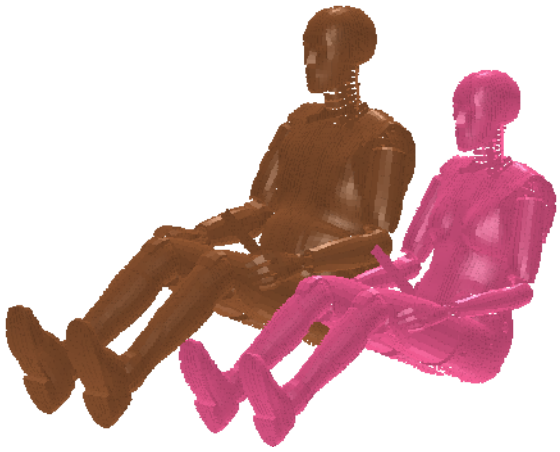

Figure 4 – Comparison EvaRID and BioRID II

the breadth dimensions in [46]. Finally, it was assumed that the EvaRID will maintain the same pelvis angle as the BioRID II at 26.5 degrees.

The scaling factor formulas are shown in Table 4 and resulting scale factors are provided in [50]. The EvaRID model is depicted in Figure 4 together with the BioRID II model.
Based on information collected on muscle tension between males and females [51] the stiffness and damping properties of discrete elements in neck and spine were scaled to a value of 70% of the original values in the BioRID II model [52].

BioRID50F DEVELOPMENT

Following the model development a prototype rear impact loading device representing 50th percentile females was constructed by modifying parts from a BioRID II dummy. Target dimensions and masses of the BioRID50F's body segments were based on the EvaRID values included in Table 3. This tool was designed to initiate studies into injury thresholds for females as it seems unlikely that data obtained for a male dummy would be appropriate for female injury risk due to the difference in size, seated posture, physical distribution and kinematics.
Generally the structure of BioRID50F is similar to BioRID II. However, some modifications were introduced to closer match the anthropometry of a 50th female. The head of the BioRID50F was made of a BioRID head from which the anterior flesh had been removed. The lower arms were shortened and the wrist rotators, wrist pivots, and hands were removed. The upper and lower legs were shortened, and the ankles were replaced by aluminium square profiles, to which the shoes were attached and the flesh was sculpted to match the reduced length of the limbs. Furthermore, sections of the interior flesh were removed and oval holes were machined in different parts of the steel skeleton to reduce mass. The spine was shortened by removing two vertebrae and reducing the height of the sacral vertebra. Two sections (one horizontal and one vertical were cut out from the torso jacket followed by the reassembly of the remaining pieces, resulting in reduced shoulder joint distance. The interface pins (connecting the spine to the torso jacket) were shortened to match the modified torso jacket width. The size of the neck and spine polyurethane bumpers was decreased and the neck muscle substitute springs were replaced by softer springs. The spring cartridges and muscle substitute wires were replaced to match the length of the new springs. Resulting masses of the BioRID II and the BioRID50F's body segments are compared in Table 5. The BioRID50F prototype loading device is shown in Figure 5. Instrumentation is similar to the BioRID [52].

Table 5 – Masses of BioRID II and BioRID50F

Dummy Segment	BioRID II Mass [kg]	BioRID50F Mass [kg]
Head	4.44	3.32
Torso (incl. neck/spine)	27.16	22.43
Pelvis	11.67	12.03
Arm (upper)	2.02	1.46
Arm (lower)	2.26	1.25
Leg (upper)	6.86	5.72
Leg (lower)	5.80	3.83
Total	**77.15**	**62.30**

Figure 5 – BioRID50F prototype loading device.

EvaRID MODEL EVALUATION

Firstly, volunteer and BioRID II hardware tests from Carlsson et al. [31] were reproduced for the initial validation of the EvaRID model. A detailed description of the test set-up, volunteers and results is given in [31] and [50]. Figure 6 compares head and T1 accelerations and rotations of the EvaRID model with corridors and Figure 7 shows results for the BioRID model plotted against corridors constructed from tests with the BioRID II hardware dummy at volunteer loading levels. Both the EvaRID and the BioRID II model showed good to reasonable correlation with test data except for the T1 rotation which remains well below test data. It should be noted that in this first validation, correction to the characteristics of discrete elements related to muscle tension was not yet made.

To allow a more detailed analysis a new series of volunteer tests was performed. In this series a rigid seat base and larger head to head-restraint distance was introduced to eliminate some of the uncertainties for the correlation with the EvaRID model. In the new

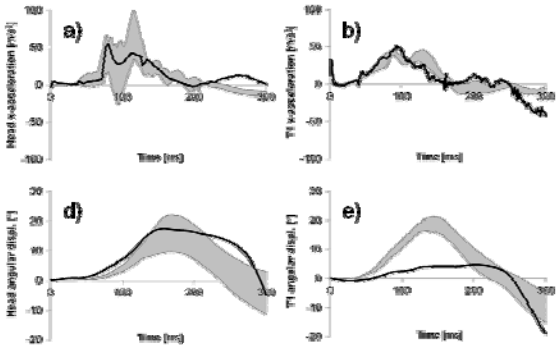

Figure 6 – Comparison of EvaRID against corridors from volunteer tests at velocity change of 7 km/h.

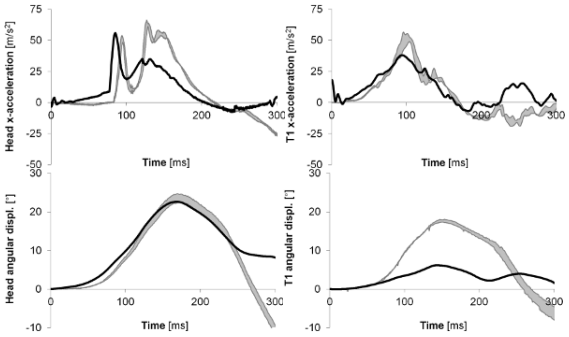

Figure 7 – Comparison of BioRID II model against corridors from hardware tests at velocity change of 7 km/h.

series tests with eight female volunteers, representing the 50th percentile female, were performed at a change of velocity of 6.8 km/h. The volunteer data are summarised in Table 6.

The set-up consisted of a stationary sled equipped with a laboratory seat designed to mimic a Volvo S80 seat [31] and [53]. This target sled was impacted from the rear by a bullet sled with an iron band mechanism dimensioned to create the mean acceleration of 2.1g of the target sled. Schematics of the test set-up can be seen in Figure 8. Dynamic response corridors for the x-accelerations, the x-displacements, and the angular displacements of the head, T1, and head relative to T1 were generated. For this purpose the head was equipped with a harness with tri-axial accelerometers mounted on the left side, and an angular accelerometer mounted on the right side, approximately at the centre of gravity of the head on each side. T1 accelerometers were mounted on a holder, which was attached to the skin at four points (one above each clavicle, and two bilateral and close to the spinal process of the T1). The volunteers were restrained by a standard three point seatbelt. See picture of volunteer in Figure 8.

The back of the seat consisted of four stiff panels, lined with a 20 mm thick layer of Tempur medium quality foam covered with a plush cloth. Panel and foam dimensions and stiffness's were derived from detailed measurements of each element. Furthermore, the stiffness of the supporting springs was derived from static measurements on each spring. The head-restraint consisted of a stiff panel and the initial Head Rest (HR) distance was adjusted to 15 cm by adding layers of padding, see Figure 8.

A pre-simulation was conducted by dropping the dummy into the seat and letting it find its balanced position in the simulation through gravity. The seat was fixed to the ground and the only external force

Table 6 – Age, stature, mass, sitting height, and neck circumference of the female volunteers

Test Subject	Age	Stat.	Mass	Sitting Height	Neck circ.
	[years]	[m]	[kg]	[m]	[m]
FA2	27	161.0	54.5	86.5	30.0
FB2		163.8	56.8	86.5	32.0
FC2	27	162.8	66.8	86.5	32.5
FD2	23	166.0	56.8	86.5	32.0
FE2	25	165.3	61.2	94.5	32.0
FF2	29	161.4	62.2	85.5	33.0
FG2	22	161.9	60.4	86.4	32.0
FH2	27	164.4	58.0	86.5	32.0
Mean	**26**	**163.3**	**59.6**	**88.6**	**31.9**
SD	**2**	**1.8**	**3.9**	**4.3**	**0.9**

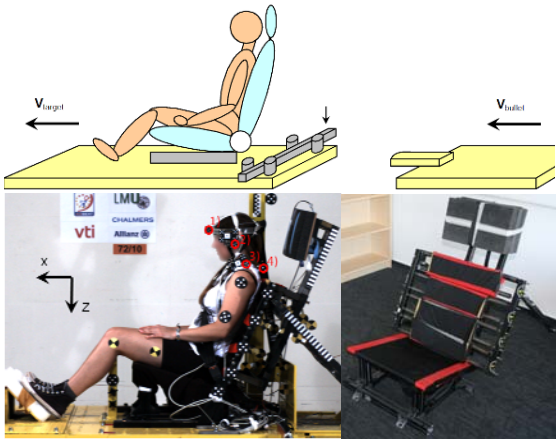

Figure 8 – Schematic of sled setup, volunteer with markers and seat with rigid seat based.

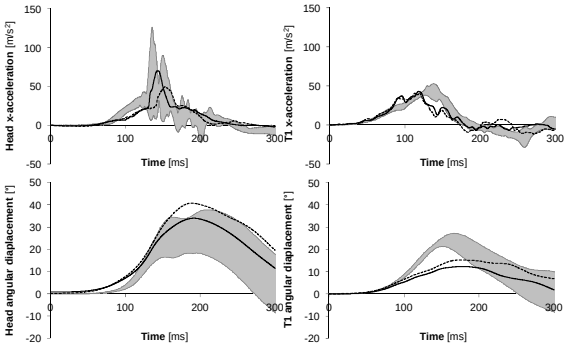

Figure 9 – Comparison of EvaRID against corridors from volunteer tests at a velocity change of 6.8 km/h.

was the gravity. The influence of dummy positioning on the seat was studied by applying a shorter and a longer run time for the pre-simulations resulting in head to headrest distances of 144 and 158 mm respectively.

Figure 9 shows some typical results. Head and T1 accelerations and angular displacements for position #1 (black line, 144 mm head-to-headrest distance) and position #2 (dotted lines, 158 mm head-to-headrest distance) compared against corridors from volunteer tests (indicated by grey lines and shaded area). Good correlation was obtained for most signals. The T1 rotation, however, remains below the corridor for the first 160 ms. Compared to results from the initial validations, improved performance was found, which is explained by clearer definition of the test conditions. This allowed for a more detailed modelling of the seat and thereby for better conditions to fine tune the EvaRID model in terms of stiffness reduction related to muscle tension.

Based on the above observations, it is advisable to further evaluate and improve the BioRID II and EvaRID models for use at low velocity changes. In this respect it is recommended to establish the curvature of the spine and its relation to the HR distance for seated 50th percentile female occupants. Such data were not available to the ADSEAT project when generating the model; therefore these results must be implemented to further improve the EvaRID model.

FEMALE NECK INJURY RISK

To apply the newly established EvaRID model in the context of seat performance assessment, it is crucial to derive parameters characterising the associated neck loading. While various criteria published to rate the male injury risk exist, of which NIC [54] and Nkm [55] are probably the most commonly applied, criteria specifically addressing the female injury risk are not yet available. Therefore, attempts were undertaken to establish initial suggestions on how to assess female injury risk. Assuming that the biomechanical basis for neck complaints is similar for male and females, injury criteria with similar underlying concepts were assumed to be appropriate. However, female specific threshold values for acceptable dynamic neck loading needed to be established.

An analysis of the Folksam Insurance data was made to compare injury risks between males and females and Figure 10 shows risk curves for both genders. From these results it was observed that the risk for females is approximately 20% higher compared to males. Kullgren et al. [6] considered a correlation between NIC and vehicle mean acceleration. Consequently, a provisional reduction of the NIC threshold value by 20%, i.e., a reduction of the

threshold value from 15 (males) to 12 (females) was suggested.
Additionally, the Nkm criterion was adapted by adjusting the intercept values used to determine the criterion. Considering a scaling approach of neck properties as described in FMVSS 208 related to the Nij criterion, as well as in Viano [21] it was suggested to reduce the intercept values for females to 60% of the corresponding values for males.

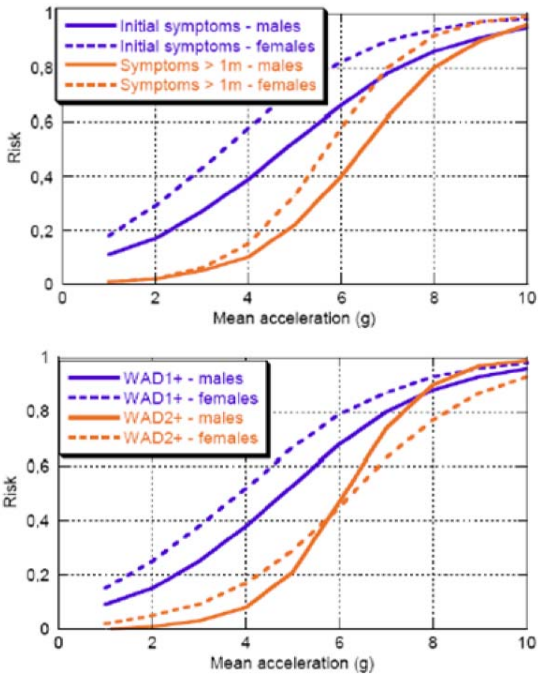

Figure 10 – Injury risk curves for males and females as derived from Folksam database.

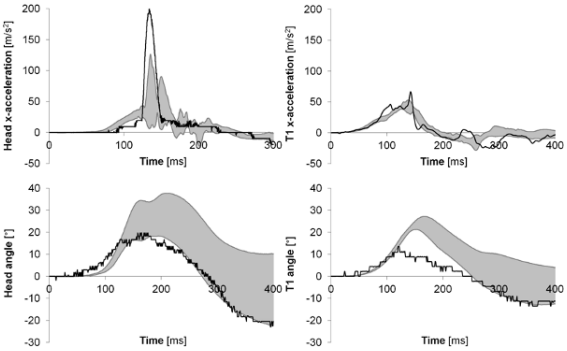

Figure 11 – Comparison of BioRID50F against corridors from volunteer tests at velocity change of 6.8 km/h.

To investigate whether these suggestions for female injury criteria are reasonable, sled tests were performed utilising the BioRID50F. Initially, the loading device was validated against the female volunteer data, see Figure 11. The overall response of the BioRID50F resembled the female volunteer response corridors. The lower thoracic and lumbar joint stiffness of the BioRID II was replicated in the BioRID50F; therefore it is possible that the spine segments were stiffer than in an average female.
Secondly, a series of sled tests adhering to Euro NCAP whiplash test procedure was performed (IIWPG 16km/h delta-v). Four commercially available vehicle seats rated by Euro NCAP were used: A, B and D awarded good rating while seat C performed marginally. Seats A and B were equipped with re-active systems to reduce the neck loading. Two seats of each model were tested, i.e., a total of 8 sled tests comprising 8 seats were performed with the new loading device BioRID50F. The tests were evaluated similar to Euro-NCAP evaluations and results are summarised in Figure 12 in terms of absolute values normalised with respect to corresponding Euro NCAP tests using the BioRID II, i.e., 1.0 representing the baseline as obtained using a BioRID.
Despite various limitations e.g., related to the new loading device, its seated posture or the seat position, the tests clearly illustrate that assessing current seats focusing on female anthropometry will lead to different results. Poorly performing seats in BioRID II tests can produce much better results under the new setting and vice versa. In seat C, for example, the smaller dummy managed to fit in between the seat frame leading to completely different kinematics associated with lower loading. Likewise, the outcome for injury criteria differed. Evaluating the modified versions of NIC and Nkm reflected the different performance of the seats as described above. Hence, it was decided to use the modified versions in the computer simulations, as well, to test their applicability to the EvaRID model.

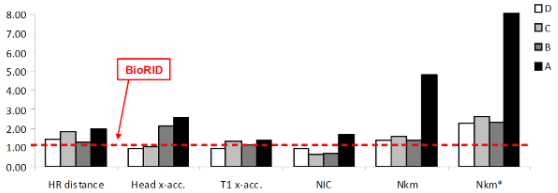

Figure 12 – Test results normalized with respect to the corresponding Euro-NCAP results.

SIMULATIONS OF VEHICLE SEATS

The new female dummy model EvaRID and limits proposed by ADSEAT were used to compare the efficacy, for males and females, of the whiplash protection systems currently on the market. Three different kinds of seats were selected to represent a wide range of typical automotive vehicle seats and head restraints. All had been awarded medium to good performance in the Euro NCAP whiplash rating.

Description of seats

The seats used in this study are shown in Figure 13. Seat A represents a middle class vehicle seat of an older generation still in serial production. The head restraint is a classic passive adjustable up/down type. Although the height in the upper most position is lower than for the latest generation of vehicle seats the dynamic performance of the seat is excellent. Seat C is a recent middle class vehicle seat awarded 3 out of the 4 possible points in the Euro NCAP whiplash rating. The headrest is adjustable up/down and has an integrated plastic insert covered by foam. Seat D is a recent vehicle seat for a small vehicle awarded 3 points in Euro NCAP ratings. This seat has an integrated head restraint at fixed height.

Seat model validation

Initially the available models for these seats were validated by comparing simulation results for the BioRID II dummy model with dummy hardware test in SRA16, IIWPG16 and SRA24 pulses. The BioRID model was positioned in line with the Euro NCAP protocol and recorded test pulses were applied.

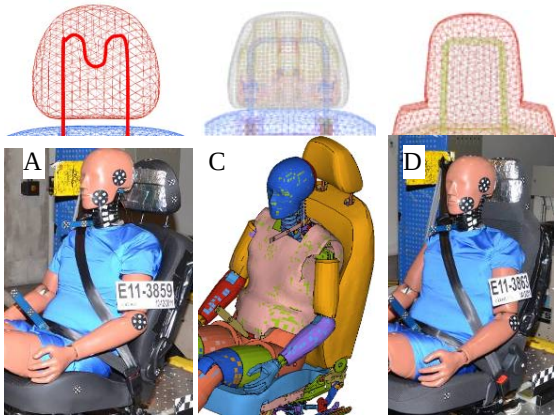

Figure 13 – Seats used in numerical study and details of the headrest.

Table 7 – Comparison of NIC and Nkm for hardware tests and simulations with the BioRID model

Seat	Pulse	NIC		Nkm	
		Test	Simu.	Test	Simu.
A	SRA16	13.01	13.65	0.23	0.16
A	IIWPG16	16.41	15.62	0.22	0.17
A	SRA24	19.86	13.26	0.35	0.27
C	SRA16	8.80	10.72	0.26	0.21
C	IIWPG16	17.99	16.35	0.24	0.17
C	SRA24	14.24	17.57	0.43	0.31
D	SRA16	9.10	10.10	0.19	0.28
D	IIWPG16	14.35	17.14	0.28	0.28
D	SRA24	14.20	19.20	0.45	0.34

A comparison was made on the basis of signals and injury criteria. Table 7 shows NIC and Nkm as an example to illustrate correlations obtained. Whereas NIC (see Table 7), Fz upper and T1 for seats A and C are comparable, the outcome on Nkm (see Table 7) and Fx differ. Also the HR contact times differ and head rebound velocities appear higher in simulation than in real test. For seat D the head contact times are aligned between FEA and the tests. Regarding the behaviour of the criteria over the time, NIC, Fx upper and T1 are the values which correlate the best between test and simulation. Head rebound velocity is again overestimated in simulations. Despite the differences observed between simulations and tests the correlations found gave sufficient confidence in applying the seat models to a comparison between the performance for males and females.

EvaRID positioning

For the simulation runs with the female dummy model it was decided not to change the seat adjustments except for the head restraint height. This allows for a comparison without any other influence factor. Where the head restraint was adjusted to the mid height position for the BioRID, it was adjusted to its lowest position for the EvaRID (see Figure 14). As no seating procedure was available the aim was to keep the EvaRID H-point in the same position as for the BioRID model. To avoid interference with the seat base the same femur orientation as for the BioRID was applied which was realised by directing the tibia in a more upward position i.e., heel further back (see Figure 15). The pelvis angle was set to 26.5+/- 2.5° (BioRID 26.5+/- 2.5°), the head angle to 0° (+/-1°) and the occiput of the EvaRID head was aligned to the occiput of the BioRID.
The seating procedure appeared to be feasible for all

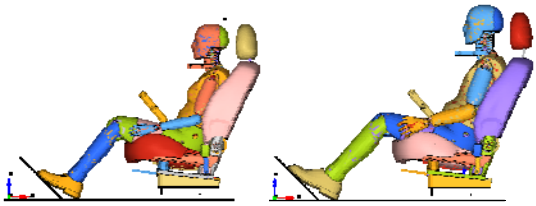

Figure 14 – Head restraint position for EvaRID (left) in lowest position and BioRID (right) in mid position.

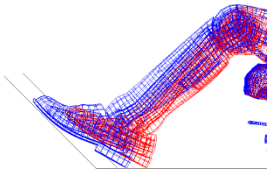

Figure 15 – Leg positioning EvaRID (red) in comparison to BioRID (blue)

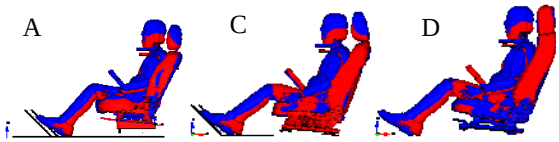

Figure 16 – Comparison of seated position for EvaRID (red) and BioRID (blue) for each seat.

seats and resulting postures and seat settings for the EvaRID in relation to the BioRID are depicted in Figure 16. Although feasible, it is to be noted that the seating procedure requires further research. Volunteer studies have shown that females and males tend to adjust the seatback differently; women´s seat back angulation being 3 degrees less than males [56].

EvaRID simulations and performance comparison for males and females

Simulations comparing the performance of the three seats for EvaRID and BioRID II were made applying the SRA16, IIWPG16 and SRA24 pulses. Figure 17 show head displacements and rotations for the IIWPG16 pulse as example. Figure 18 and Figure 19 provide results for NIC and Nkm respectively. Notable differences were observed for seat D. This is explained by the fact that the EvaRID head is not contained by the headrest due to lack of support; firm support is missing at the contact location between the occiput and the headrest for the female dummy. When considering the thresholds for NIC (12) and Nkm as identified for the EvaRID it is evident that all seats perform better for the BioRID than for the EvaRID.

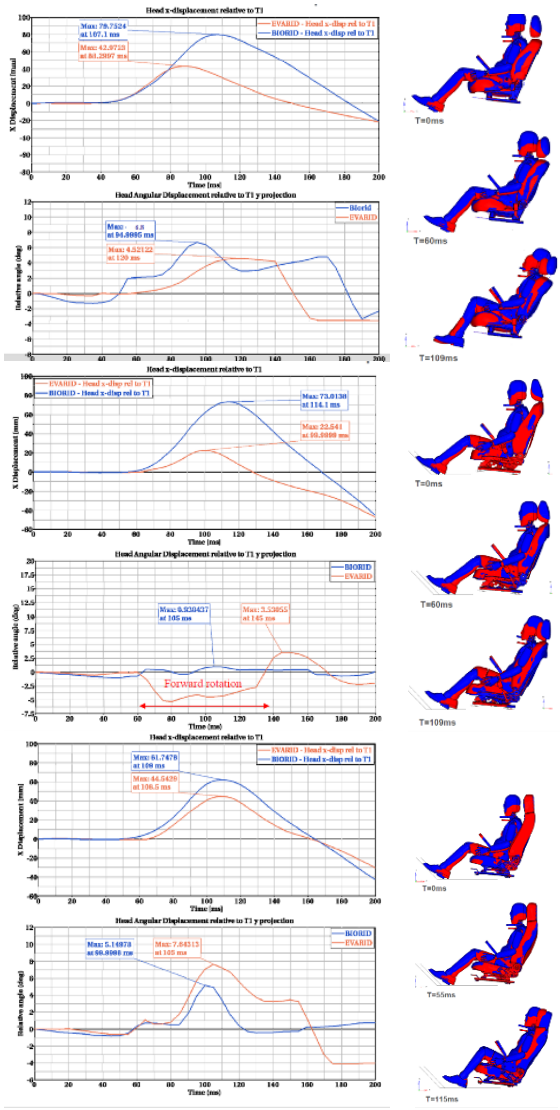

Figure 17 – Head x displacements and relative angles for EvaRID (red) and BioRID (bleu) for IIWPG16 pulse: seat A (top); seat C (middle) and seat D (bottom)

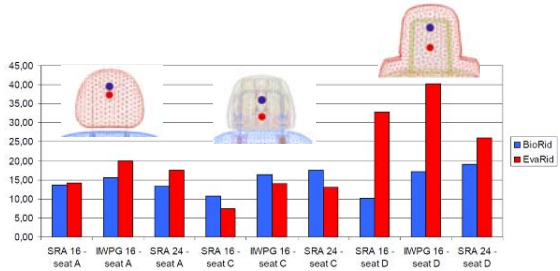

Figure 18 – NIC values for EvaRID (red) and BioRID II (blue) in three different seats and at three different pulses. Contact point between head and headrest indicated for each seat.

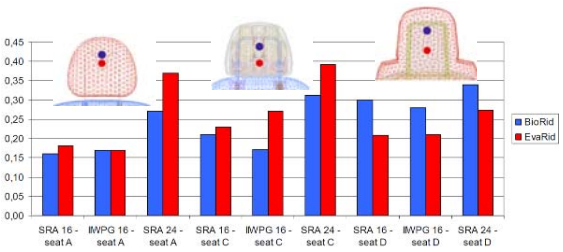

Figure 19 – Nkm for EvaRID (red) and BioRID II (blue) in three different seats and at three different pulses. Contact point between head and headrest indicated for each seat.

DISCUSSION

Real-world car crash records shows that females have a higher risk of sustaining whiplash injuries, than males. An analysis of insurance data conducted in the ADSEAT project showed that females associated with the highest whiplash injury frequency in rear impacts are of average size [33]. Related anthropometry data were collected and used to scale an available BioRID II model. The resulting model, called EvaRID, is meant to represent females in rear impact studies. The EvaRID model was validated against two sets of response corridors obtained from female volunteer tests. Despite a reasonably good overall correlation the EvaRID model showed a notably low T1 rotation compared to the volunteer data from the first test series, see Figure 6. Comparison between the BioRID II model and hardware tests in the same conditions showed identical behaviour, see Figure 7. The results suggest that the biofidelity of both the EvaRID and the BioRID II model have limitations at low velocity changes in the range of 7 km/h. This may be explained by the fact that the BioRID II model is mostly used and therefore largely validated against dummy test results in the range of consumer test load conditions.

In the second series of female volunteer tests a seat with rigid base and larger head to head restraint distance was applied allowing for more accurate reproduction in simulations. In this condition better correlation was obtained although the T1 rotation remained below the corridors, see Figure 9.

Based on these observations it is recommended to further evaluate and improve the virtual BioRID II and EvaRID models for performance in low velocity changes. In this respect it is advisable to establish the curvature of the spine and its relation to the HR distance for seated 50th percentile female occupants in the EvaRID. Such data were not available to the ADSEAT project when generating the model.

For the injury criteria and thresholds to be used with the EvaRID model it was assumed that the biomechanical basis for soft tissue neck injuries is similar for male and females. As a consequence criteria previously established for the BioRID II were adopted. A comparison of injury risks between males and females [6] indicates that the risk for females is approximately 20% higher compared to males. On this basis a reduction of the NIC threshold value by 20% was proposed as a first estimate. For the Nkm reduced intercept values of 29 Nm for extension moment, 53 Nm for flexion moment and 507 N for shear force for females were proposed. These values are based on a scaling approach of neck properties as described in FMVSS 208 (related to the Nij criterion) as well as a publication by Viano [21] which would suggest reducing the intercept values for females to 60% of the corresponding values for males.

The appropriateness of these thresholds was investigated by sled tests comparing the performance of seats using the BioRID II dummy and a newly established loading device called BioRID50F. The BioRID50F was developed by modifying components from the BioRID II to make a closer match to the anthropometry of the 50th percentile female. Comparative tests on four different production seats revealed differences in outcome of the tests due to the differences in anthropometry of both loading devices. In one of the seats the smaller dummy managed to fit in between the seat frame leading to completely different kinematics resulting in lower values of the neck loadings. Evaluation of the adopted thresholds for NIC and Nkm reflected the differences in behaviour. Although the approach applied has many limitations including the correctness of the loading device applied and the lack of an adequate seating procedure it was decided to use the proposed lowered values for NIC and Nkm for the EvaRID model. However, further work in this field is much needed.

Simulations with production seats using the BioRID II and the EvaRID model showed that significant differences may occur between the response of the BioRID II and EvaRID models. As seat and headrest designs respond to actual consumer procedures which favour a mid-height position of the head restraint at the height of the BioRID II dummy, the EvaRID response may suffer in those situations where the head cannot be fully retained by the head restraint due to lack of support. The head restraint needs to provide firm support at the height of the occipital point of the average female. This could for

instance be realised by adding additional inserts within the head restraint or alternatively by allowing the head restraint to be aligned with the top of the head of the EvaRID. The real world data and the research findings in the ADSEAT project are expected to become essential input for future updates of test protocols such as IIHS and Euro NCAP. In terms of usage of the EvaRID model it is to be noted that future studies into the seat adjustments and seating procedure for females are required to reflect for the fact that females tend to apply different seat adjustments than males [56].

CONCLUSION

A computational dummy model, called EvaRID, Eva female, RID – Rear Impact Dummy, of a 50th percentile female for use in rear impact tests was developed based on anthropometry data found in the literature. To evaluate how close the dummy model´s response was to that of a human, the EvaRID was compared to the corridors and response curves gained in volunteer tests comprising females. Good overall correlation was found except for the T1 rotation, indicating that further refinement to the spine geometry is needed possibly in conjunction with stiffness optimisation to achieve a response fully within the corridors.

With respect to injury criteria it was concluded that it would be appropriate to begin by using NIC (with a lower threshold value of 12 m2/s2) and Nkm (with reduced intercept values of 29 Nm for extension moment, 53 Nm for flexion moment and 507 N for shear force for females). Evaluation of these values using a new experimental loading device called BioRID50F reflected the different behaviour observed in tests comparing seat performance for the BioRID50F and the BioRID II. The same was true for simulations comparing seat performance for males and females using the EvaRID and the BioRID models. Further work in this field is needed though.

Virtual impact simulations with seats showed that for some seats significant differences may occur between the response of the BioRID II and EvaRID model. The initial results of the simulations showed that in similar conditions the female occupant behaves less favourably in terms of loading to the neck, than male occupants. To improve the validity of such simulations a seating procedure including related tools, specifically for females are to be developed.

ACKNOWLEDGEMENT

This study was funded by the European Commission within the 7th Framework Programme. Additional funding has been received from the Swedish Transport Agency.

REFERENCES

[1] Kullgren A, Krafft M, Lie A, Tingvall C (2007) The Effect of Whiplash Protection Systems in Real-Life Crashes and Their Correlation to Consumer Crash Test Programmes, Proc. 20th ESV Conf. (07-0468), Lyon (France), pp. 1–7

[2] The Whiplash Commission Final Report (2005) http://www.whiplashkommissionen.se/pdf/WK_final report.pdf

[3] Nygren A (1984) Injuries to Car Occupants - Some Aspects of the Interior Safety of Cars, Acta Oto - Laryngologica - Supp1. 395, ISSN 0365-5237

[4] Galasko CSB, Murray PA, Pitcher M (1996) Whiplash Associated Disorders, Proc. 15th ESV Conf., Melbourne (Australia), pp. 1504–1513

[5] Eichberger A, Geigl BC, Moser A, Fachbach B, Steffan H (1996) Comparison of Different Car Seats Regarding Head-Neck Kinematics of Volunteers During Rear End Impact, Proc. IRCOBI Conf., Brunnen (Switzerland), pp. 153–164

[6] Kullgren A, Eriksson L, Boström O, Krafft M (2003) Validation of neck injury criteria using reconstructed real-life rear-end crashes with recorded crash pulses, Proc. 18th ESV Conf.

[7] Watanabe Y, Ichikawa H, Kayama O, Ono, K, Kaneoka K, Inami S (2000) Influence of seat characteristics on occupant motion in low-velocity rear-end impacts, Accid. Anal. Prev., Vol. 32, No. 2.

[8] Kihlberg JK (1969) Flexion-Torsion Neck Injury in Rear Impacts, Proc. 13th AAAM, pp. 1–16

[9] Thomas C, Faverjon G, Hartemann F, Tarriere C, Patel A, Got C (1982) Protection against Rear-End Accidents, Proc. IRCOBI Conf., Cologne.

[10] Maag U, Desjardins D, Bourbeau R, Laberge-Nadeau C (1990) Seat Belts and Neck Injuries, Proc. IRCOBI Conf., Bron (France), pp. 1–14

[11] Morris AP, Thomas PD (1996) Neck Injuries in the UK Co-operative Crash Injury Study, Proc. 40th Stapp Car Crash Conf., SAE 962433), pp. 317–329

[12] Dolinis J (1997) Risk Factors for “Whiplash” in Drivers: a Cohort Study of Rear-End Traffic Crashes, Injury, Vol. 28, No. 3, pp. 173–179

[13] Temming J, Zobel R (1998) Frequency and Risk of Cervical Spine Distortion Injuries in Passenger Car Accidents: Significance of Human

Factors Data, Proc. IRCOBI Conf., Göteborg (Sweden).
[14] Chapline JF, Ferguson SA, Lillis RP, Lund AK, Williams AF (2000) Neck pain and head restraint position relative to the driver's head in rear-end collisions, Accid. Anal. Prev., Vol 32, No. 2.
[15] Krafft M, Kullgren A, Lie A, Tingvall C (2003) The Risk of Whiplash Injury in the Rear Seat Compared to the Front Seat in Rear Impacts, Traffic Inj. Prev., Vol. 4, No. 2, pp. 136–140
[16] Jakobsson, L (2004) Field Analysis of AIS1 Neck Injuries in Rear-End Car Impacts-Injury Reducing Effect of the WHIPS Seat, J. of Whiplash & Related Disorders, Vol. 3, No. 2, pp. 37–54
[17] Storvik SG, Stemper BD, Yoganandan N, Pintar FA (2009) Population-Based Estimates of Whiplash Injury Using NASS CDS Data, Biomed Sci Instrum., No. 45, pp. 244–249
[18] Carstensen TB, Frostholm L, Oernboel E, Kongsted A, Kasch H, Jensen TS, Fink P (2011) Are There Gender Differences in Coping with Neck Pain Following Acute Whiplash Trauma? A 12-Month Follow-Up Study, Eur. J. Pain, Vol. 16, No. 1.
[19] Svensson MY, Lövsund P, Håland Y, Larsson S (1993) Rear-end collisions—A study of the influence of backrest properties on head–neck motion using a new dummy neck, SAE/SP-93/963, Warrendale.
[20] Croft AC, Haneline MT, Freeman MD (2002) Differential Occupant Kinematics and Forces Between Frontal and Rear Automobile Impacts at Low Speed: Evidence for a Differential Injury Risk, Proc. IRCOBI Conf., Munich (Germany).
[21] Viano D (2003) Seat Influences on Female Neck Responses in Rear Crashes: A Reason Why Women Have Higher Whiplash Rates, Traffic Inj. Prev., Vol. 4, No. 3, pp. 228–239
[22] Szabo TJ, Welcher JB, Anderson RD, Rice MM, Ward JA, Paulo LR, Carpenter NJ (1994) Human Occupant Kinematic Response to Low-Speed Rear End Impacts, Proc. 38th Stapp Car Crash Conference
[23] Siegmund GP, King DJ, Lawrence JM, Wheeler JB, Brault JR, Smith TA (1997) Head/Neck Kinematic Response of Human Subjects in Low-Speed Rear-End Collisions, Proc. 41st Stapp Car Crash Conf., SAE 973341, pp. 357–385
[24] Hell W, Langwieder K, Walz F, Muser M, Kramer M, Hartwig E (1999) Consequences for Seat Design due to Rear End Accident Analysis, Sled Tests and Possible Test Criteria for Reducing Cervical Spine Injuries after Rear-End Collision, Proc. IRCOBI Conf., Sitges (Spain), pp. 243–259
[25] Welcher JB, Szabo JS (2001) Relationships between Seat Properties and Human Subject Kinematics in Rear Impact Tests, Accid. Anal. Prev., Vol. 33, No. 3, pp. 289–304
[26] Mordaka J, Gentle RC (2003) The Biomechanics of Gender Difference and Whiplash Injury: Designing Safer Car Seats for Women, Acta Politechnica, pp. 47–54
[27] Ono K, Ejima S, Suzuki Y, Kaneoka K, Fukushima M, Ujihashi S (2006) Prediction of Neck Injury Risk Based on the Analysis of Localized Cervical Vertebral Motion of Human Volunteers During Low-Speed Rear Impacts. Proc. IRCOBI Conf., Madrid (Spain), pp. 103–113
[28] Linder A, Carlsson A, Svensson MY, Siegmund GP (2008) Dynamic Responses of Female and Male Volunteers in Rear Impacts, Traffic Inj. Prev., Vol. 9, No. 6, pp. 592–599
[29] Schick S, Horion S, Thorsteinsdottir K, Hell W (2008) Differences and Commons in Kinetic Parameters of Male and Female Volunteers in Low Speed Rear End Impacts, TÜV SÜD, Whiplash – Neck Pain in Car Crashes, 2nd Intern. Conf., Erding
[30] Carlsson A, Siegmund GP, Linder A, Svensson M (2010) Motion of the Head and Neck of Female and Male Volunteers in Rear Impact Car-to-Car Tests at 4 and 8 km/h, Proc. IRCOBI Conf., Hanover
[31] Carlsson A, Linder A, Davidsson J, Hell W, Schick S, Svensson M (2011) Dynamic Kinematic Responses of Female Volunteers in Rear Impacts and Comparison to Previous Male Volunteer Tests, Traffic Inj Prev. Vol. 12, pp. 347–357
[32] Welsh R, Lenard J (2001) Male and Female Car Drivers – Differences in Collision and Injury Risks, Proc. 45th AAAM, Texas (USA), pp. 73–91
[33] Kullgren A, Krafft M (2010) Gender analysis on whiplash seat effectiveness: Results from real-world crashes, Proc. IRCOBI Conf., Hanover (Germany)
[34] Carlsson A (2012). Addressing Female Whiplash Injury Protection - A Step Towards 50th Percentile Female Rear Impact Occupant Models. Göteborg: Chalmers University of Technology. ISBN/ISSN: 978-91-7385-671-3
[35] Linder A, Schick S, Hell W, Svensson M, Carlsson A, Lemmen P, Schmitt K-U, Tomasch E. (2012) ADSEAT – Adaptive Seat to Reduce Neck Injuries for Female and Male Occupants. TRA Conference, 23-26 April, Athens, Greece.
[36] Temming J, Zobel R (1998) Frequency and Risk of Cervical Spine Distortion Injuries in Passenger Car Accidents: Significance of Human Factors Data, Proc. IRCOBI Conf., Göteborg (Sweden).

[37] Jakobsson L, Lundell B, Norin H, Isaksson-Hellman I (2000) WHIPS-Volvo's Whiplash Protection Study, Accid. Anal. Prev., Vol. 32, No. 2.
[38] Linder A, Olsén S, Eriksson J, Svensson MY, Carlsson A (2012) Influence of Gender, Height, Weight, Age, Seated Position and Collision Site related to Neck Pain Symptoms in Rear End Impacts, Proceedings: IRCOBI Conference; September 12-14; Trinity College, Dublin, Ireland
[39] Jakobsson L., Norin H., AIS1 Neck injury reducing effect of WHIPS (Whiplash Protection System), Proceedings IRCOBI Conference 2004
[40] Hanson L, Sperling L, Gard G, Ipsen S, Olivares Vergara C (2008) Swedish anthropometrics for product and workplace design, Appl Ergon., Vol. 40.
[41] Moss S, Wang Z, Salloum M, Reed M, van Ratingen M, Beusenberg M (2000) Anthropometry for WorldSID a World-Harmonized Midsize Male Side Impact Crash Dummy, SAE Paper No. 220-01-2202, Warrendale, PA, USA
[42] Schneider LW, Robbins DH, Pflüg MA and Snyder RG. Development of Anthropometrically Based Design Specifications for an Advanced Adult Anthropomorphic Dummy Family. Final Report, UMTRI-83-53-1; University of Michigan Transportation Research Institute; 1983; Ann Arbor
[43] Robbins DH. Anthropometric Specifications for Mid-Sized Male Dummy. Final Report, UMTRI-83-53-2; University of Michigan Transportation Research Institute; 1983; Ann Arbor, Michigan, USA
[44] Robbins DH. Anthropometric Specifications for Small Female and Large Male Dummies. Final Report, UMTRI-83-53-3; University of Michigan Transportation Research Institute; 1983
[45] Diffrient N, Tilley AR, Bardagjy JC. Humanscale 1/2/3 – A Portfolio of Information. The MIT Press; 1974; Cambridge, MA
[46] Young JW, Chandler RF, Snow CC, Robinette KM, Zehner GF, Lofberg MS. Anthropometric and Mass Distribution Characteristics of Adult Female Body Segments. Federal Aviation Administration, Civil Aeromedical Institute; 1983; Oklahoma, USA
[47] Cheng H, Obergefell L, Rizer A. Generator of Body (GEBOD) Manual. Report No. AL/CF-TR-1994-0051; 1994; Human Effectiveness Directorate, Crew Surviability and Logistics Division, Write-Patterson Air Force Base, Ohio, USA
[48] Seidl A. RAMSIS – A New CAD Tool for Ergonomic Analysis of Vehicles Developed for the German Automotive Industry. SAE Paper No. 970088; 1997; Society of Automotive Engineers, Inc., Warrendale, PA, USA
[49] McConville JT, Churchill TD, Kaleps I, Clauser CE, Cuzzi. Anthropometric Relationships of Body and Body Segment Moments of Inertia. AMRL-TR-80-119; 1980; Wright-Patterson AFB, Aerospace Medical Research Laboratory, Yellow Springs, USA
[50] Carlsson A, Chang F, Lemmen P, Kullgren A, Schmitt K-U, Linder A, Svensson MY. EvaRID – A 50th Percentile Female Rear Impact Finite Element Dummy Model, Proceedings: IRCOBI Conference; September 12-14; Trinity College, Dublin, Ireland
[51] Foust DR, Chaffin DB, Snyder RG, Baum JK (1973) Cervical Range of Motion and Dynamic Response and Strength of Cervical Muscles, Proc. 17th Stapp Car Crash Conf., Society of Automotive Engineers (730975), Warrendale, PA (USA).
[52] Stahlschmidt S, Keding B, Witowski K, Müllerschön H, Franz U (2006) BioRID-II dummy model development – stochastic investigations, The 5th German LS-DYNA Forum; Ulm, Germany
[53] Davidsson J, Deutscher C, Hell W, Svensson MY, Linder A, Lövsund P (1998) Human Volunteer Kinematics in Rear-End Sled Collisions, Proc. IRCOBI Conf., Göteborg (Sweden), pp. 289–301
[54] Boström O, Svensson M, Aldman B, Hansson H, Håland Y, Lövsund P, Seeman T, Suneson A, Säljö A, Örtengren T (1996) A new neck injury criterion candidate based on injury findings in the cervical spinal ganglia after experimental neck extension trauma, Proc. IRCOBI Conf., pp. 123-136
[55] Schmitt K-U, Muser M, Walz F, Niederer P (2002) Nkm — a proposal for a neck protection criterion for low speed rear-end impacts, Traffic Injury Prevention, Vol. 3 (2), pp. 117-126
[56] Jonsson B, Stenlund H, Svensson MY, Björnstig U (2008) Seat adjustment – capacity and repeatability among occupants in a modern car, Ergonomics, Vol. 51, No. 2, pp. 232–4